Charles University
Faculty of Science

Study programme: Geology
Branch of study: Applied Geology

Bc. Kateřina Bočková

Change of clay fill structure induced by applied stress

Přeměna struktury jílových výsypek vlivem působícího napětí

Master's thesis

Supervisor: RNDr. Jan Najser, Ph.D.

Prague, 2021

Prohlášení:

Prohlašuji, že jsem závěrečnou práci zpracovala samostatně a že jsem uvedla všechny použité informační zdroje a literaturu. Tato práce ani její podstatná část nebyla předložena k získání jiného nebo stejného akademického titulu.

V Praze, 19.05.2021

Kateřina Bočková

Acknowledgment

My sincere gratitude goes to the thesis supervisor RNDr. Jan Najser, Ph.D., for his expert and constructive guidance, and assistance in conducting laboratory tests, especially the physical models.

Secondly, I would like to thank GeoTec-GS, a.s. for the permission to use the data from the research project in this thesis.

And last but not least, I would like to thank my colleague and friend Bc. Anna Vilimová for her support, help with the laboratory tests, and numerous beneficial discussions about the research topic.

Abstract

The open-cast brown coal mining in Northwestern Bohemia produces vast amounts of a lumpy clayey material dredged from the overlying sedimentary layers and deposited into large landfills (clay fills). The clay fills are typical for their double porosity (inside and between lumps), which, when related to the absence of artificial compaction, results in their open and metastable structure. Their structural transition from a coarse-graded (lumpy) material into a fine-graded material (reconstituted clay) is influenced by time, degree of saturation, and stress.

The structural transition of Bílina Clay Fill, induced by applied stress, is studied by two scaled-down physical models. Their isotropic compressibility and hydraulic conductivity are tested in a large triaxial cell under increasing stress. A series of standard laboratory tests in a small triaxial cell and oedometer on reconstituted and undisturbed samples provides the limiting characteristic values to the possible behavior of the models.

The results showed that the hydraulic conductivity of a saturated clay fill non-linearly decreases as the macrovoids close, approaching the hydraulic conductivity of a reconstituted soil at 540 kPa of the vertical effective stress. Then the macrovoids are filled with the reconstituted soil only, and the trend becomes linear. On the other hand, the compressibility is at lower stresses (on a semi-logarithmic scale) linear. Up to the vertical effective stress in a range between 4 and 4.6 MPa, the clay fill behaves as a slightly overconsolidated soil due to the presence of lumps. Then it reaches the compressibility of a reconstituted soil.

Abstrakt

V severozápadních Čechách probíhá rozsáhlá povrchová těžba hnědého uhlí. Nadložní jílovité vrstvy jsou odtěžovány a ve formě hrud ukládány na výsypky. Pro tyto výsypky je typická jejich dvojí pórovitost (uvnitř hrud a mezi nimi). V souvislosti s absencí zhutňování, vede tato dvojí pórovitost k otevřené metastabilní struktuře výsypek. Přeměna struktury výsypky z hrubozrnné (hroudovité) na jemnozrnnou (rekonstituovaný jíl) je závislá na čase, stupni nasycení a napětí.

Přeměna struktury vnitřní výsypky dolu Bílina vlivem napětí je zkoumána pomocí dvou fyzikálních modelů výsypky s redukovanou zrnitostní distribucí hrud. Změna stlačitelnosti a hydraulické vodivosti modelů je testována při zvyšujícím se napětí ve velké triaxiální komoře. Zkoušky na neporušených vzorcích poskytly doplňující informace o mechanickém chování překonsolidované zeminy, tvořící jednotlivé hroudy. Cílem zkoušek na rekonstituovaném materiálu bylo stanovení referenčních hodnot pro charakterizaci výsypky s plně degradovanou původní strukturou.

Výsledky ukázaly, že hydraulická vodivost nasycené výsypky nelineárně klesá v souvislosti s postupně se uzavírajícími makropóry. Při vertikálním efektivním napětí 540 kPa se hodnota hydraulické vodivosti dostane na hodnotu hydraulické vodivosti rekonstituované zeminy. Makropóry jsou pak vyplněny pouze rekonstituovanou zeminou a při zvyšujícím se napětí je již změna hydraulické vodivosti lineární. Stlačitelnost nasycené výsypky je (v semilogaritmickém grafu) lineární už při nízkých napětích. Kvůli přetrvávající přítomnosti hrud se výsypka chová jako mírně překonsolidovaná zemina až do vertikálního efektivního napětí v rozsahu 4 – 4.6 MPa. Po dosažení tohoto napětí odpovídá svou stlačitelností rekonstituované zemině.

1. Contents

List of Figures

List of Tables

List of Symbols

A	pore pressure coefficient
A	cross-sectional area of the sample
A_c	area after the consolidation
B	pore pressure coefficients
c_v	coefficient of consolidation
c_{vi}	coefficient of consolidation for isotropic consolidation
e	void ratio
e_e	intergranular void ratio
e_i	intragranular void ratio
e_t	total void ratio
e_1	void ratio at the beginning of the loading stage
δe	change in void ratio during the loading stage
f_{cv}	multiplying factor
H	height of the sample
H_0	height of the sample at the beginning of the test
ΔH	axial deformations, cumulative settlement
H_c	height of the sample after the consolidation
Δh	settlement (height change)
i	hydraulic gradient
I_p	plasticity index
k	hydraulic conductivity
K_0	coefficient of earth pressure at rest
L	length of the drainage path (sample's height)
m_d	dry mass of soil
m_v	coefficient of volume compressibility for oedometric consolidation
m_{vi}	coefficient of volume compressibility for isotropic consolidation
m_w	mass of water
N	location of isotropic normal compression line in $(1+e)$:lnp' space
n_e	intergranular porosity
n_i	intragranular porosity
n_t	total porosity
P	axial force
p'	mean effective stress
$\delta p'$	effective stress increment

Q	rate of flow
q	deviator stress
s'	center of the effective Mohr circle
t	time
t'	radius of the effective Mohr circle
t_{50}	time corresponding to 50 % of primary consolidation
T_{50}	time factor
u	pore pressure
Δu	pore pressure difference between the top and bottom base of the sample
v	mean discharge velocity of flow of water in soil
V_t	total volume
V_p	volume of pores
V_s	volume of soil grains
ΔV	volume change
w	water content
w_n	natural water content
w_P	plastic limit
w_L	liquid limit
γ	unit weight
ε_a	axial strain
λ	gradient of the compression line
ρ_s	particle density
σ'	normal effective stress
σ'_v	vertical effective stress
σ_3	minor principal stress (cell pressure)
σ'_3	minor effective principal stress
σ'_1	major effective principal stress
τ'	shear effective stress
φ'_{cr}	critical state angle of friction

1. Introduction

Tertiary basins in Northwestern Bohemia are rich in brown coal, which is extensively mined in open-cast mines. The overlying sedimentary layers of about 150 m in thickness are composed mostly of lacustrine clays and claystones. During the mining, the clays are excavated and deposited in a form of lumps into spoil heaps, thus creating landfills over 100 m high (Feda, 1998). For such a kind of landfill, the term ‘clay fill’ or ‘fill’ is used in this thesis. As the area occupied by clay fills increases, the need to utilize their surface for construction purposes is growing.

Clay fill is a typical example of an artificially created soil of a double porosity: porosity inside the lumps and between each other. Their deposition is carried out without any artificial compaction; therefore, the fill acquires an open and metastable structure, which makes the fill more prone to collapse. In addition, the significant heterogeneity of clay fill in time and space can be observed; it results in differential settlements of the fill. Therefore, the understanding of its behavior is challenging while crucial for the safety of the construction.

The leading factor of the clay fill’s mechanical behavior is its structural transition from a coarse-graded material formed by lumps to a fine-graded material with behavior similar to a reconstituted clay. The transition is mainly influenced by time, degree of saturation, and stress. Those three factors are strongly interconnected. However, this thesis focuses primarily on the effect of stress.

The thesis aims to describe the process of the structural transition of the saturated clay fill induced by the applied stress. For this purpose, two physical models of Bílina Clay Fill are created from the lumps of Libkovice Member and tested in the large triaxial cell. The observed parameters accompanying the structural changes with the increasing pressure include the change of volume (consolidation and compressibility) and hydraulic conductivity. The limiting behavior of the models is defined by the characteristics of the excavated overconsolidated clay on one side and by the characteristics of the reconstituted clay representing a fully degraded clay fill on the other side. Such reference characteristics are determined by a series of standard laboratory tests in a small triaxial cell and an oedometer on undisturbed and reconstituted samples.

2. Clay fills

The clays removed from their natural deposits are in the form of lumps stored in a new place. The artificially structured soil created from the dredged clayey lumps is called clay fill. A typical feature of clay fills is their double porosity (see Fig. 2.1). The lumps, mostly composed of stiff to hard clay, behave as a granular material during their deposition and create voids (also known as macrovoids) between themselves. Moreover, the lumps preserve the inner porosity of the original clay (also known as microvoids). Feda (1998) specified the porosity of a granular character of the fresh fill as intergranular (n_e, e_e) and the porosity of the intact lumps as intragranular (n_i, e_i). The resulting total porosity n_t (%) and the total void ratio e_t (-) can be calculated as:

$$n_t = n_i(1 - n_e) + n_e \tag{1}$$

$$e_t = e_i(1 + e_e) + e_e \tag{2}$$

The double porosity results in a very high overall porosity and an open metastable structure of the clay fill. This often results in large settlements and the risk of sudden collapses. Over time, as the fill degrades, the structure changes from coarse lumpy clay back into the more homogenous clay. The understanding of the clay fill's behavior is thus essential for its exploitation.

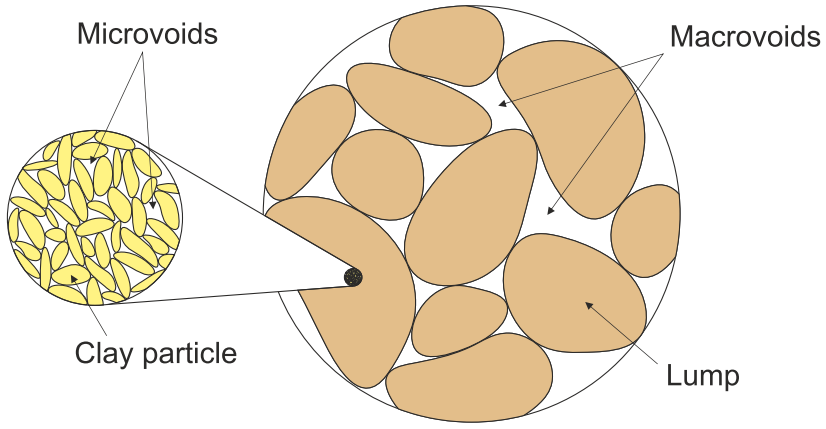

Fig. 2.1 Double porosity of clay fill.

There are two main types of clay fills that the current research focuses on:

- DREDGED UNDER AND FILLED INTO THE WATER
- DREDGED AND FILLED IN THE OPEN-CAST MINES

The first type mentioned usually develops as a product of construction works at the sea bottom and is used in land reclamation as an alternative to costly sand. Its behavior slightly differs from the second one and is described in chapter 2.1. The clay fill of the open cast mine is a waste product of mining and is stored in the fills. The closer description is in chapter 2.2.

These two types of clay fills are not generally compacted. However, the dredged clayey lumps can be, in the form of compacted fill, used as a construction element in earth dams, road embankments, or backfill below or within structures. Their behavior was studied, for example, by Cox (1979). Nevertheless, the compacted or so-called engineered clay fills are out of the scope of this thesis.

2.1. Filling into the water

The creation of an artificial land from the water is one of the forms of land reclamation. For this purpose, a clay fill dredged usually from the water body's bottom can be used. Clayey lumps up to 2 m in size are dumped onto the island seabed and form a landfill (Karthikeyan, et al., 2004). The large initial macrovoids are filled with water and small clay lumps. The presence of water decreases the matric suction, and thereby the degradation is accelerated. Before the surcharge is applied, the lumps undergo softening due to unloading and swelling, which decreases their strength and stiffness (Dortland, 2019). Consequently, preloading even to the low pressure (25 kPa) closes up the macrovoids, which are then filled with the homogenized clay composed of degraded small lumps and outer shells of big lumps. The fill then undergoes substantial settlement (Leung, et al., 2001), as shown in Fig. 2.2. The associated behavior (the rate of consolidation and hydraulic conductivity), up to the preconsolidation pressure, is then derived from the characteristics of the reconstituted clay. On the other hand, the compressibility is primarily governed by the lump characteristics. Above the preconsolidation pressure, the influence of the lumps vanishes, and the fill becomes homogenized.

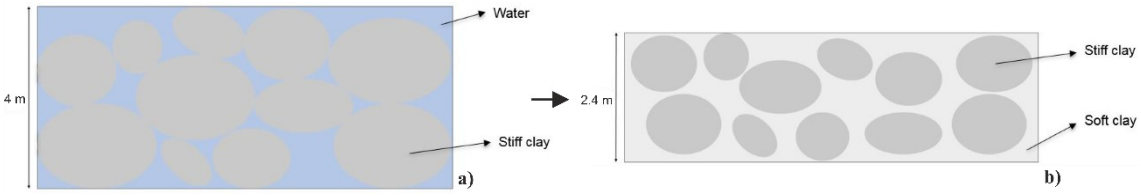

Fig. 2.2 Change of the structure by preloading (Dortland, 2019).

Many studies have been done on the topic of filling into the water using clayey lumps. For example, in Singapore by Leung, et al. (2001), Yang, et al. (2002), Li-Ang (2003), Jun Wei (2004), Karthikeyan, et al. (2004), and Robinson, et al. (2005), in India by Juneja & Chafale (2018), and in the Netherlands by Dortland (2019). The following section presents several of them.

Leung, et al. (2001) examined the behavior of clay balls (simulating the fill lumps) in a large one-dimensional compression apparatus and in a centrifuge. The authors found out that the presence of macrovoids results in a faster rate of consolidation and a higher hydraulic conductivity of the fill than that of the homogenous clay at the same loading pressure. As the loading pressure is increasing, the macrovoids are closing up, and the difference diminishes. However, the overall settlement of the fill is larger compared to the homogenous clay. Furthermore, due to the denser packing, the fill consisting of spherically shaped lumps settles less than the fill of lumps cubically or irregularly shaped.

In his PhD thesis, Jun Wei (2004) studied the consolidation and compressibility of clay fill. He carried out two sets of laboratory experiments. The first one was testing the softening behavior of single lumps, from which he concluded that the larger lumps soften slower than smaller lumps and that the water content of the fully softened lumps can be even close to the liquid limit. In the second set, he performed large one-dimensional consolidation tests on cubical lumps and slurries of various consistencies (for comparison). The more softened the lumps were, the smaller were the macrovoids, and the lower was their compressibility. Also, he observed that the rate of consolidation and the hydraulic conductivity of clay fill are governed by the material filling the macrovoids. This material has little effect on compressibility.

Karthikeyan, et al. (2004) performed a site investigation of a 12 years old reclaimed island in Singapore. Using the radioisotope cone penetration test and laboratory experiments, they tested the strength and deformation of the reclaimed land. The size of macrovoids was reduced to the microvoid size, although the clay fill was still heterogeneous. The density, strength, and deformation were highly variable with normally consolidated and overconsolidated zones. The coefficient of secondary compression was similar to that of the homogenous clay. They stated the clay fill is a suitable material for land creation.

Robinson, et al. (2005) have done a series of consolidation tests on a clay fill made of cubical lumps. They investigated the influence of lump size, initial packing

arrangement, and the effect of degree of swelling on the clay fill's strength and hydraulic conductivity. They determined that the influence of the lump size and the packing arrangement is negligible when compared to the influence of swelling. At the consolidation pressure of 100 kPa, they observed the decrease of hydraulic conductivity to the values of a homogenous clay. The determined coefficient of secondary compression was similar to that of the normally consolidated clay, suggesting that the secondary compression does not play an important role. Furthermore, they found the shear strength of a fill ranging between the strengths observed in normally consolidated and overconsolidated clays. After reaching the preconsolidation pressure of the lumps, the shear strength became uniform with depth.

Dortland (2019), in his master thesis, studied the factors influencing the clay fill's macrovoids closure. He carried out experimental swell-load tests on an overconsolidated clay, CT images of discontinuities, and a test on a fill made of clay balls in a Rowe cell. He identified the softening due to swelling as a dominant factor of the macrovoids closure. The studied influence of pore water chemism showed the increasing expansive strains with the decreasing salinity. Also, the larger initial suction resulted in more significant swelling. Furthermore, he observed the effect of hydraulic conductivity on the softening time but not on the final strains.

2.2. Clay fills of open-cast mines

During the open-cast coal mining, a significant amount of waste material is produced. To expose the coal seam, the overlying sedimentary layers (mostly clays and claystones) are excavated. The excavated material is transported in the form of lumps and placed on spoil heaps creating clay fills.

The lumps retain natural water content at ca. 30 % and porosity at ca. 40 % of the original clay (Feda, 1998). Their degree of saturation is close or equal to 1, but the macrovoids in between them remain dry. As a result, the suction at the contacts can be neglected. However, the matric suction inside the lumps is significant due to unloading by excavation (Herbstová & Herle, 2009). The total porosity of such a material is about 70 % (Feda, 1998).

The filling process, according to Najser (2010), results in the heterogeneous lump distribution. The finer material remains in the center of the heap, but the bigger lumps

roll down and accumulate at the toe. Therefore, the character of the fill varies not only in time but also in space.

The clay fill exposed to climate effects and overburden pressure decomposes in time from the originally granular lumpy material into a practically homogenous water-saturated clay. The structural transition process is highly dependent on applied stress (load), degree of saturation (water content), and time (Feda, 1998). The original clay is strengthened by overconsolidation; therefore, the process may take many years (Herbstová & Herle, 2009), as shown in Fig. 2.3. Charles (2008) described a case study on the long-term behavior of open cast mining clay fills in the UK. He stated that the poorly compacted backfills are likely to be metastable and sensitive to disturbance independently on the fill's age.

Fig. 2.3 Clay fill during the filling a) and clay fill 10 – 15 years old b) (Najser, 2010).

According to Kostkanová, et al. (2014), the lumps flooded at the natural water content remain practically intact. On the other hand, the exposure to the wetting-drying cycles and the accompanying suction oscillations results in their easier disintegration. A similar observation was reported by Shi & Herle (2014), as shown in Fig. 2.4.

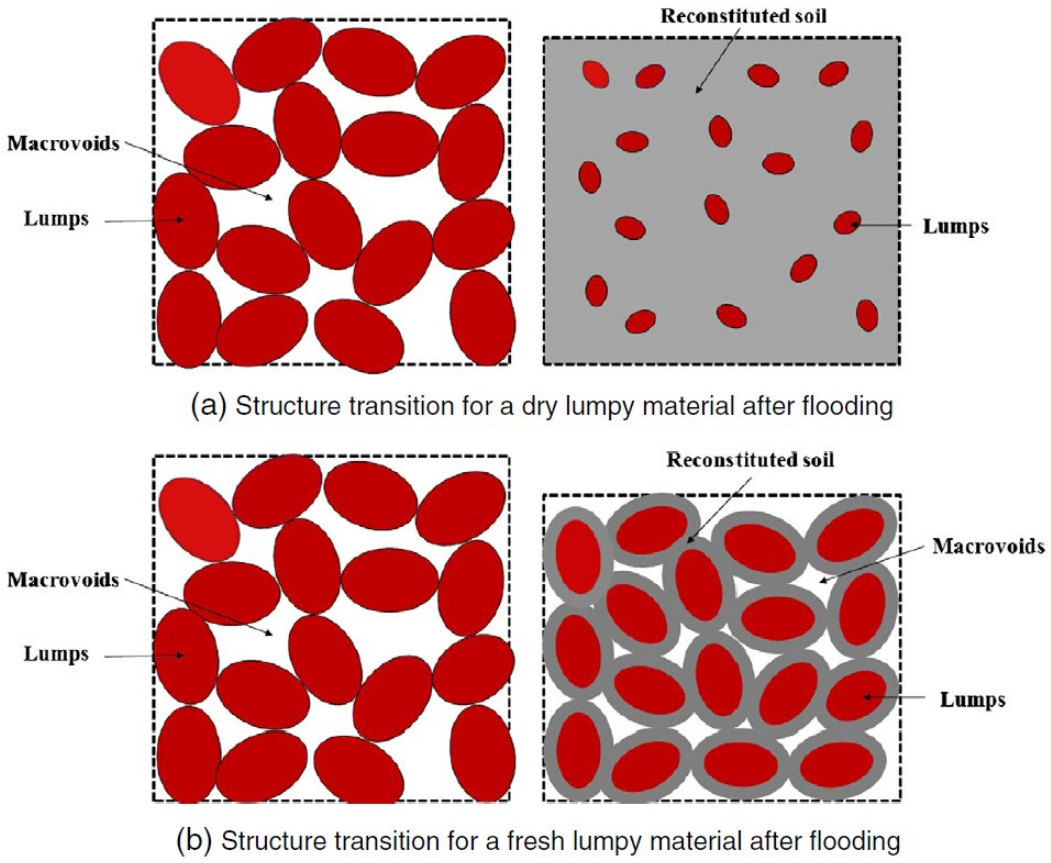

Fig. 2.4 Comparison of the structural transition after flooding a) the dried lumps, and b) naturally wet lumps (Shi & Herle, 2014).

In this thesis, the dry fill should be regarded as a fill composed of oven-dried lumps, the wet fill as a fill of lumps at the natural water content and macrovoids filled with air, and the saturated fill as a fill where all the voids are filled with water.

Several authors were studying the behavior of open cast mining clay fills, for example Feda (1998), Herbstová & Herle (2009), Karpíšková (2009), Najser, et al. (2010), Najser (2010), Kostkanová (2011), Kostkanová, et al. (2014), Shi & Herle (2014). Most of these studies were focusing on the clay fills in Northwestern Bohemia. This chapter summarizes their findings.

2.2.1. Mechanisms of structural transformation

Feda (1998) characterizes four mechanisms of structural transition:

- **Crushing** of clayey lumps. Crushing is a brittle intragranular deformation. The compression curve of a clay fill being crushed has a garlandlike form (see curves 3 and 4 in Fig. 2.8). The wet clay lumps are weaker than the dry lumps; therefore, they are more likely to be crushed. The crushing of

lumps is the same as the crushing of grains and is more comprehensively described by Feda (1982).

- **Squashing** of wet lumps (Fig. 2.5 bottom right). The lumps are compressed and deformed in a ductile manner (not disintegrated). This results in strain hardening as the void size reduces.
- Lump **rearrangement** (Fig. 2.5 bottom left). The lumps are mutually sliding and rotating, which leads to densification and strain hardening.
- **Contact bonding**. Wet clay lumps stick one to another. The apparent bonds are reducing the compression and restrain the rearrangement.

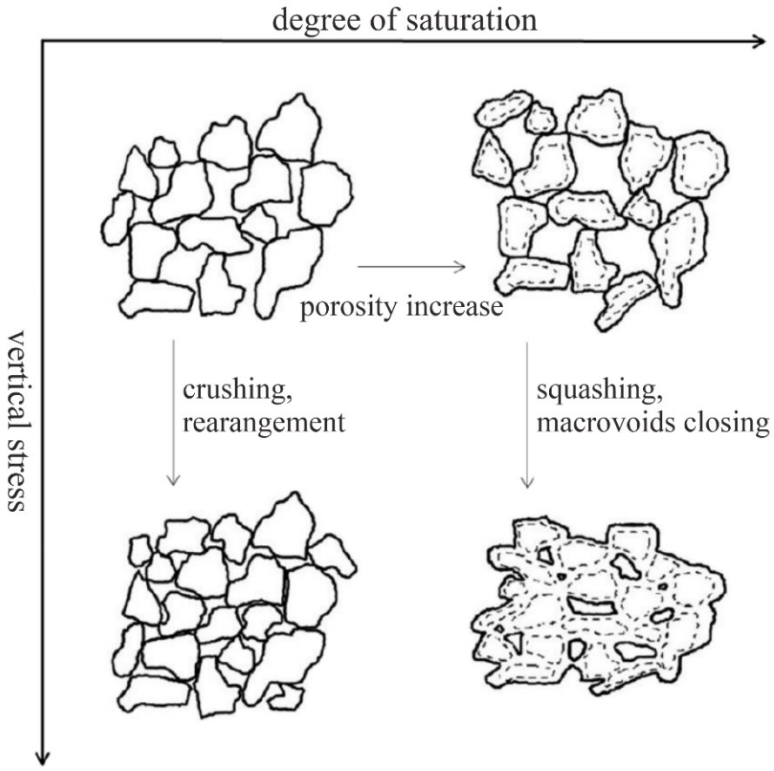

Fig. 2.5 Structural transitions of the clay fill at different degrees of saturation when the vertical stress is applied (after Najser, et al. (2010)).

At small depths (low pressures), shortly after the filling, the structure is open, and the macrovoids are dry (Fig. 2.5 top left), thus being collapsible and highly permeable. The leading transformation behavior is the rearranging and eventually crushing of lumps. With increasing pressure, crushing becomes more significant (Fig. 2.5 bottom left). As time is passing, the clay fill close to the surface is slowly being saturated by the rainfall. The wetting-drying cycles induced by the weather change the matric suction, which leads to the disintegration of lumps that subsequently fills the macrovoids (Herbstová & Herle,

2009). On the other hand, as the clay fill close to the surface transforms to more homogenous clay, wetting-drying cycles can create new preferential paths similar to desiccation cracks so that the hydraulic conductivity stays high. As a result, the macrovoids of the consolidated clay fill are connected to a certain depth (10 to 15 m according to Najser, et al. (2010), 12.5 to 25 m according to Karpíšková (2009)).

In the lower parts of the clay fill (high pressures), the lumps are under the weight of the overburden squashing into the macrovoids, which results in their closure (Fig. 2.5 bottom right). The complete macrovoid closure of the wet fill was determined at the threshold of 1500 kPa (corresponding to 75 m of overburden) by Herbstová & Herle (2009). The saturation of the clay fill at greater depths is primarily caused by the free water level increase.

Shi & Herle (2014) divide the structural transition of the saturated clay fill into three stages according to the stress level *p'*:

- **The first stage** at which the stress is lower than the threshold for the closure of macrovoids. The clay fill consists of three phases: voids filled with water and reconstituted soil, and lumps.
- **The second stage**, where the stress ranges between the threshold and preconsolidation pressure. All the macrovoids are filled with the reconstituted soil only. The structure is still highly heterogeneous.
- **The third stage**, where the stress level exceeds the preconsolidation pressure and the clay fill becomes homogeneous.

However, as the softening and hydraulic conductivity changes are gradual, the thresholds are represented by stress ranges rather than single values.

For a double porosity material with the metastable structure, such as clay fill, the collapsible behavior is typical. For example, when mining is finished, the mining company terminates water pumping in the mine area, the water level rises, and the relatively quick flooding results in hydrocollapse of the inner fill. In general, collapse is a sudden transformation of structural configuration, which results in a change of behavior. Feda (1998) describes the collapses of clay fill based on his laboratory experiments. The most typical are:

- **Hydrocollapse**, caused by particle disintegration due to the matric suction vanishment accompanying the dry or wet fill flooding.
- **Immediate collapse** is the result of compression of dry and wet fill. It takes place immediately after the surcharge.

2.2.2. Hydraulic conductivity

Hydraulic conductivity is dependent on the clay fill's structure and the interconnected macrovoids. With the structural changes and the consequent closure of macrovoids, the hydraulic conductivity decreases by several orders of magnitude (Kostkanová, et al., 2014).

At the first stage after Shi & Herle (2014) (i.e., before the macrovoids closure), the hydraulic conductivity is controlled by macrovoids, and the relationship with stress is (on the logarithmic scale) linear (see Fig. 2.6). During the second stage, the leading component is the reconstituted soil filling the macrovoids and the relationship is non-linear. In both stages, the values of hydraulic conductivity are higher for a clay fill than for a homogenous clay under the same consolidation stresses due to the higher hydraulic conductivity of the soil in macrovoids. After reaching the third stage, the clay fill's hydraulic conductivity coincides with the reconstituted soil's hydraulic conductivity, and the relationship is linear again. The relationship between hydraulic conductivity and the void ratio of clay fill is linear (as for the reconstituted soil) for all three stages (Shi & Herle, 2014).

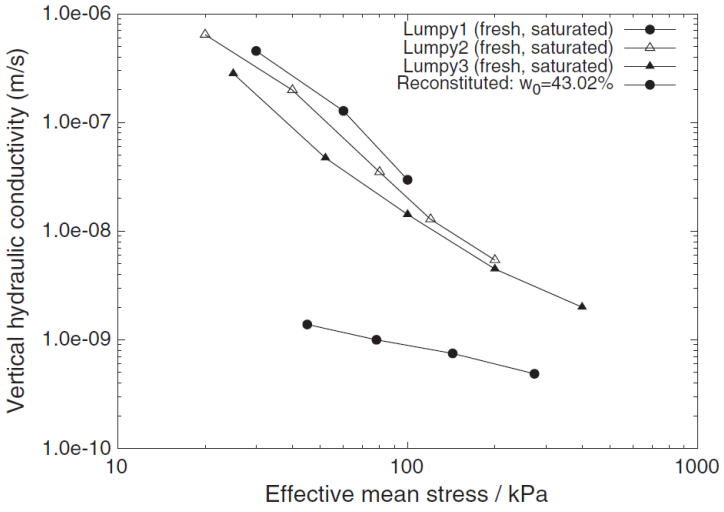

Fig. 2.6 Hydraulic conductivity of isotropically compressed clay fill samples and reconstituted soil (Shi & Herle, 2014).

The hydraulic conductivity also might be time-dependent. Kostkanová (2011) stated that the creep of lumps' contacts affects the hydraulic conductivity. After a month of loading at 60 kPa, the hydraulic conductivity of her model sample dropped by three orders of magnitude. Therefore, the hydraulic conductivity of a clay fill may not be constant in time.

2.2.3. Consolidation

The rate of consolidation is strongly affected by the hydraulic conductivity of the material. When the porosity is high, the water can easily drain through the interconnected macrovoids, and the material can consolidate quickly. On the other hand, the material with low hydraulic conductivity resists the drainage and consolidates slowly.

Consolidation curves of flooded fills have a typical S shape (see Fig. 2.7). The wet fills, especially at low pressures, consolidate extremely fast, as the macrovoids are connected and filled with air. As the macrovoids close, the consolidation becomes slower, and the consolidation curve shape of a wet fill is getting closer to the typical one. However, after a certain time span, the deformation accelerates into the secondary creep, which might be interpreted as a time-dependent collapse (Herbstová & Herle, 2009).

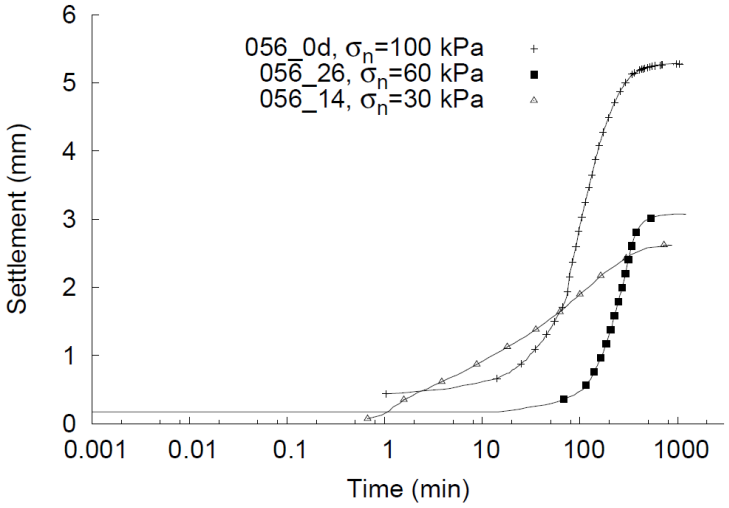

Fig. 2.7 Consolidation curves of flooded clay fill sample (Kostkanová, 2011).

In the Shi & Herle's (2014) second stage, the porosities of lumps and reconstituted soil in macrovoids are different. The resulting gradient of the excess pore pressure between them accelerates the lumps' consolidation.

2.2.4. Compressibility

The structural mechanism governing the compression depends on the stress level and water content (suction). Fig. 2.8 presents the compression curves of lumpy clay samples subjected to one-dimensional compression at various degrees of saturation measured by Feda (1998). In the semi-logarithmic plot, the saturated sample (1) shows the linear compression trend common for the reconstituted samples. The compression curve of the dry specimen (2) has (in a linear plot) a bilinear character, representing the elastoplastic compression. The fragment crushing is governing the compression of dry (3) and wet (4) samples, with the typical garlandlike trend.

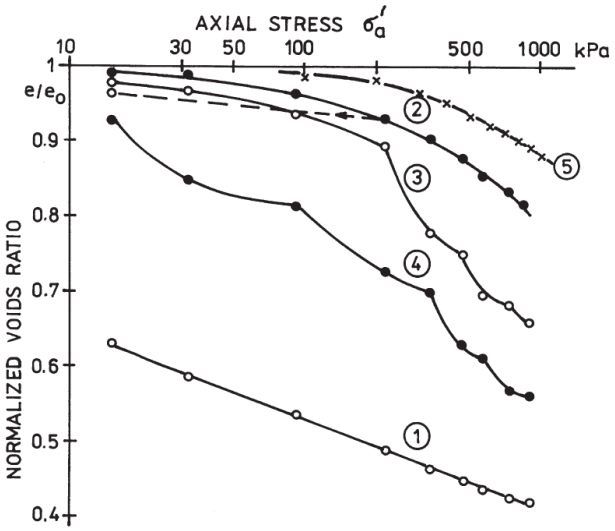

Fig. 2.8 Compression curves of clay fill with different water content: 1) saturated, 2) dry, 3) dry (crushing prevailing), 4) wet, and 5) natural intact clay (Feda, 1998).

From the studies of Herbstová & Herle (2009) and Shi & Herle (2014), it is clear that the position of the compression line/curve relative to NCL (normal compression line) depends on the clay fill's initial state. The compression curve of the wet fill lies above the NCL due to the higher strength of lumps caused by the matric suction and diagenetic bonds. Also, dry lumps preserve the structure even under high pressures. On the contrary, the compression line of a flooded fill lies below the NCL, as the open structure has already collapsed after flooding, and the lumps are squeezing into macrovoids. It combines the deformation of a highly compressible reconstituted soil in macrovoids, and a low compressible lump remains (see Fig. 2.4 top right); thus, the total porosity is smaller than for the reconstituted soil. At high stresses, as the clay fill homogenizes, the compression lines/curves converge to NCL.

In situ, the compressibility of a clay fill after the first surcharge is high and non-uniform (Najser, et al., 2010). It is the highest in the top part, where the macrovoids are the largest.

2.2.5. Strength

Stress is concentrated into the lump contacts; therefore, the strength of the fill is highly dependent on their resistance. The strength of the lumps indicates how high load the clay fill skeleton is able to carry before its brittle or ductile deformation starts. It is influenced by matric suction, overconsolidation, and in some cases by diagenetic processes as well. Herbstová & Herle (2009) measured the uniaxial compressive strength of clayey lumps from Bílina mine. It ranged between 0.53 and 1.06 MPa, which almost corresponds to the uniaxial strength of weak rocks. Therefore, the lumps composing the Bílina clay fill are ranging between stiff clays and weak claystones. When the fill is saturated, the shear strength declines given the decrease in matric suction, which reduces the strength of lumps and shear resistance at their contacts.

According to Feda (1998), the water content is the governing factor of the clay fill's shear behavior (Fig. 2.9). Multilinearity of the strength envelope is a result of structural mechanism transformation with increasing stress. At low stress, the main structural mechanism is the lump rearrangement. When the level of stress is high, the behavior is governed by crushing and interlocking for a dry clay fill and sticking and squashing for a wet clay fill, which corresponds to the compression behavior.

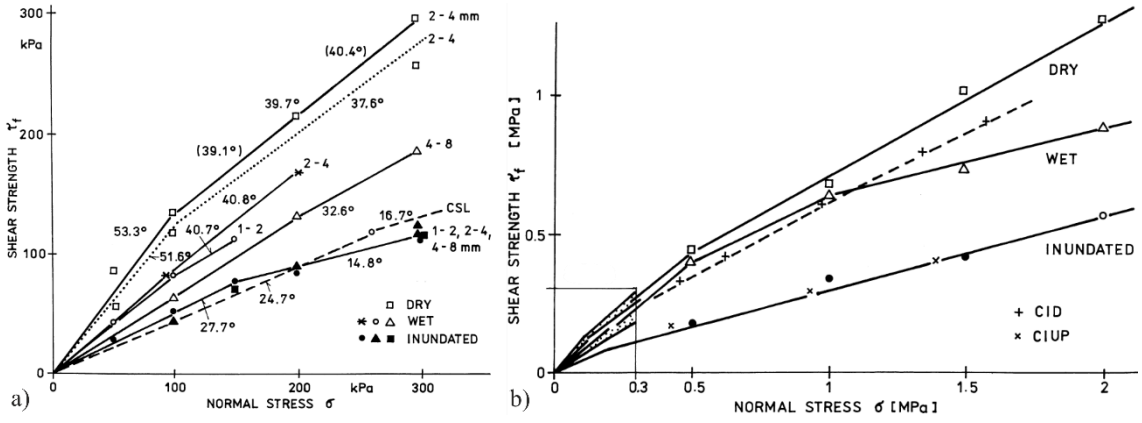

Fig. 2.9 Shear strength envelopes of clay fill at a) low, b) high stress level (Feda, 1998).

In the Shi & Herle's (2014) first and second stages, the shear strength of the saturated clay fill is controlled by the reconstituted soil around the lumps and in the macrovoids, respectively. Therefore, in the critical state, the strengths of a saturated clay

fill and a homogenized clay are comparable, which correlates with Feda's (1998) experiments (see Fig. 2.9 a, where the inundated sample and the reconstituted soil marked by dashed line have similar strength envelopes).

2.3. Numerical modeling

Several authors modeled the behavior of clay fills. For example, Yang, et al. (2002) modeled the consolidation of a clay fill using the dual porosity model for a fissured clay with the effect of self-weight included. Li-Ang (2003) developed the dual-spring model based on the double porosity concept, formulated an analytical solution, and derived the finite element program solving the non-linear equations. Mašín (2007) developed a hypoplastic model for clay with a meta-stable structure based on the principle of sensitivity by Cotecchia & Chandler (2000). Najser, et al. (2012) used Mašín's (2007) model to study the behavior of clay fills. Finally, Shi, et al. (2017) proposed a consolidation model of a clay fill material based on the concept of double porosity and the homogenization theory. However, a more profound discussion of constitutive models is beyond the scope of this thesis.

3. Locality of interest

3.1. Most Basin

The Most Basin is a Tertiary basin located in Northwestern Bohemia. It is the largest sub-basin out of five sub-basins in the Eger (Ohře) Graben, separated by volcanic elevations and fault systems (see Fig. 3.1). The basin's deposition took place from the latest Eocene to the latest Early Miocene (Rajchl, et al., 2008).

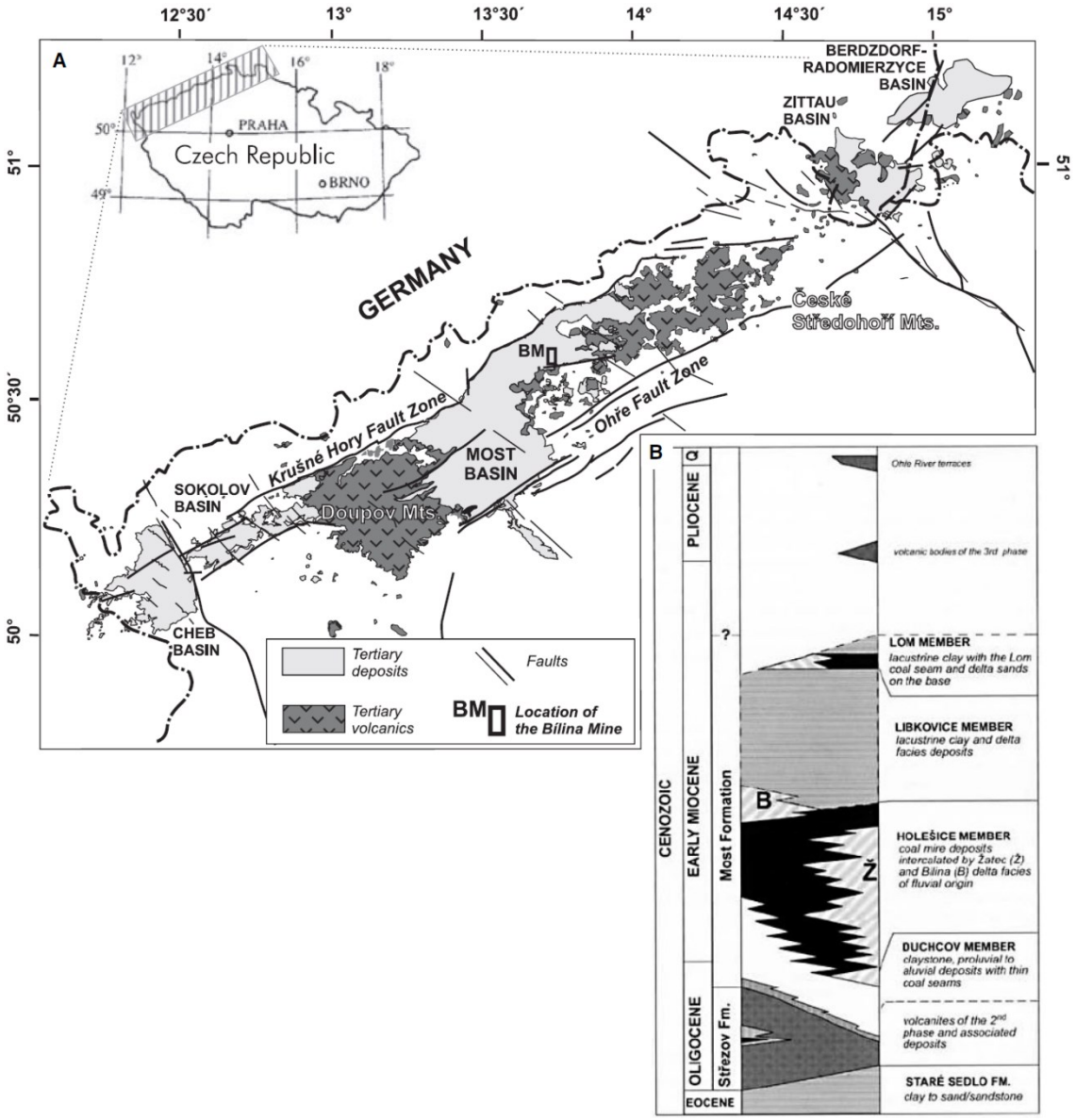

Fig. 3.1 A) Map of Tertiary basins within the Eger (Ohře) Graben (Rajchl, et al., 2008). B) Stratigraphy of the Most Basin (Kvaček, et al., 2004).

The overall sedimentary infill exceeds 500 m and is assigned to the Most Formation (Kvaček, et al., 2004). The formation is interpreted as a lacustrine-fluvial system, being divided into four members: the underlying Duchcov Member, Holešice Member with the main seam, and two delta sediment formations (Žatec and Bílina delta), overlying Libkovice Member (lacustrine clay), and Lom Member with the minor seam.

The following description of listed members is based on Kvaček, et al. (2004):

Duchcov Member – During the Duchcov Member deposition, the basin was a flat land with stagnant-water lakes. Krušné hory Mountains did not exist at that time, and the basin's subsidence was very slow. The weathered products transported by streams constituted the filling material.

Holešice Member – As the subsidence increased, the flooded area and the flatland with swamps and shallow lakes spread. The accumulation of plant biomass was rather occasional. Then, a stream entered the basin at Žatec, creating the delta (composed of sand and clay). A stable inflow resulted in an accumulation of plant biomass being in equilibrium with groundwater level increase and a peat layer up to 200 m thick (the future coal seam up to 50 m thick) deposited. The orogenetic processes, uplifting the Krušné hory Mountains, shifted the stream from Žatec to Bílina, leading to Bílina Delta development.

Libkovice Member – As the basin subsided, stream from Bílina progressively flooded the basin and formed a large shallow lake (1 – 7 m deep). The subsequent deposition of clays buried the peat layer.

Lom Member – When the deepening slowed down, the lake shallowed, and the accumulation of plant biomass was re-established, creating a thin Lom Seam.

The sediments of Libkovice Member (studied in this thesis) are monotonic lacustrine silty clays. During the deposition, they reached a thickness of about 300 m (Mach, 2002). After the sedimentation of the uppermost Lom Member, a significant extent of erosion took place in the Most Basin. The reconstruction of the overlying complex by Hurník (1978) showed that the original thickness of the basin (up to 550 m) was reduced due to the post-sedimentary denudation by about 70 to 300 m. Therefore, a significant level of overconsolidation of the sediments is present.

3.2. Bílina Mine

Bílina Mine, located in the Most Basin (see Fig. 3.1 A), is the deepest (200 m) open cast mine in the Czech Republic (Herbstová & Herle, 2009). Exposing its 25 – 40 m thick brown coal seam, about 150 m of the overlying clays and claystones are excavated. These Neogene clays of high plasticity (typically the liquid limit of 73 to 94 % and plasticity index up to 60 %) and natural water content at about 30 % are characterized as illite-kaolinitic with an admixture of montmorillonite and siderite and silty particles of quartz (Feda, 1998; Kostkanová, 2011).

During the mining process, the dredged material in the form of lumps up to 0.5 m in size (Feda, 1998) is transported by belt conveyors and deposited with sowing machines with a rotating boom firstly into the outer fills (at the beginning of mining) and then into the inner fills, where the material fills the hole created by mining. Due to the vast amount of the excavated material, no artificial compaction takes place. However, the lumps are partially compacted by a free fall from the boom (Najser, 2010).

4. Characterization of samples

All the examined material originates from Libkovice Member of Bílina mine. The material used to create the physical models (61441) was sampled directly from the belt conveyor. Unfortunately, its exact origin is not known, as the material is mixed during the transportation. The aim was to compare the behavior of the model material with a similar soil of the same origin. From a large number of samples sampled in the Bílina mine, two (59296 and 60386) were selected based on the similar plasticity and grain size distribution to sample 61441. Both were sampled from drill holes (see Fig. 4.1).

The examinations described in this chapter were performed by the commercial laboratory SG Geotechnika a.s. and the geotechnical company GeoTec-GS, a.s.

Fig. 4.1 Ortophoto map of Bílina mine. Sampling locations highlighted by purple and pink circles (satellite imagery by Mapy.cz (2019)).

To create a physical model, the knowledge of a particle (lumpy) size distribution curve of a newly developed fragmentary soil was necessary. To determine it, the belt conveyor transporting a freshly dredged clay was declined, and several tons of the material poured aside. Each lump with size exceeding 10 cm was measured by hand in

the mine. The lumps were sorted according to their size into the fractions and weighted. From the natural water content, the dry weight of lumps was calculated. The size distribution of finer particles was determined by sieving in a laboratory. Before sieving, the material was dried under 60°C (to prevent mineralogical damage) until reaching equilibrium. The resulting curve is presented in Fig. 4.2.

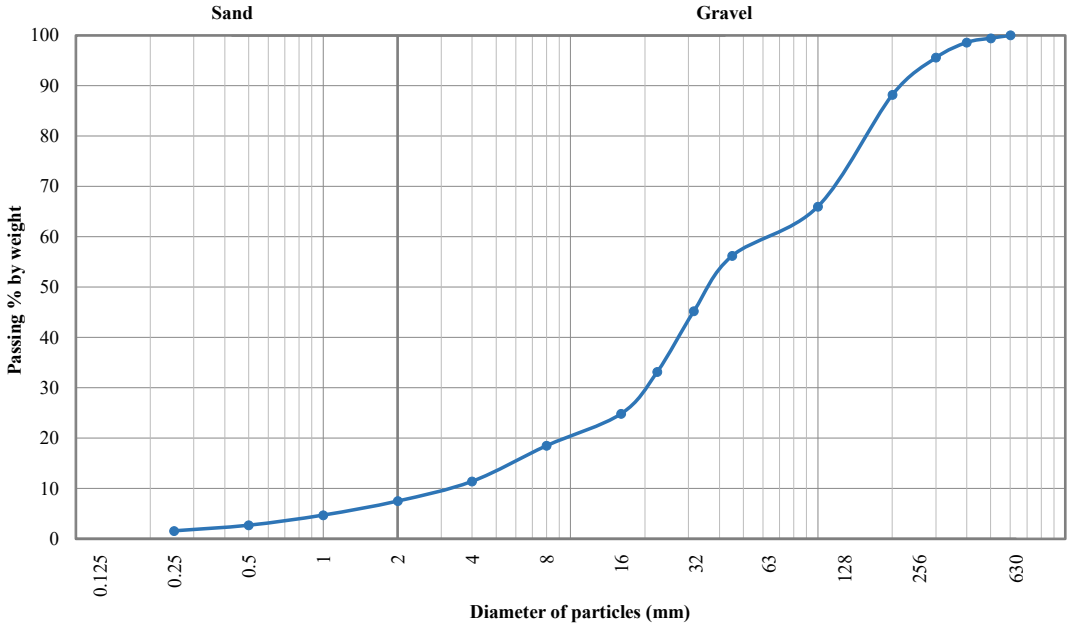

Fig. 4.2 Particle size distribution curve of a fresh clay fill.

The lump material was described as a very stiff, gray, high plasticity silty clay. Part of the dried and sieved material was remolded and used to determine index properties (sample number 61441). The particle size distribution curve (Fig. 4.3) indicates the sample's composition of 40 % clay, 50 % silt, and 10 % sand.

Sample number 59296 was sampled at a depth of 22.5 – 22.9 m from a drill hole located in a mining foreground (Fig. 4.1). It is a natural soil characterized as a hard, brown-gray, high plasticity silty clay. The particle size distribution curve, presented in Fig. 4.3, displays the sample's composition of 48 % clay, 50 % silt, and 2 % fine sand.

Sample number 60386 was sampled from a drill hole in an inner fill (Fig. 4.1). Considering a depth of 138.7 – 139.0 m, it most likely represents the bottom part of the fill. This clay fill material is characterized as a hard, brown, high plasticity clay, composed of 56 % clay, 39.4 % silt, and 4.6 % sand (see Fig. 4.3).

Index properties of the samples are summarized in Table 4.1. Fig. 4.4 presents the plasticity chart.

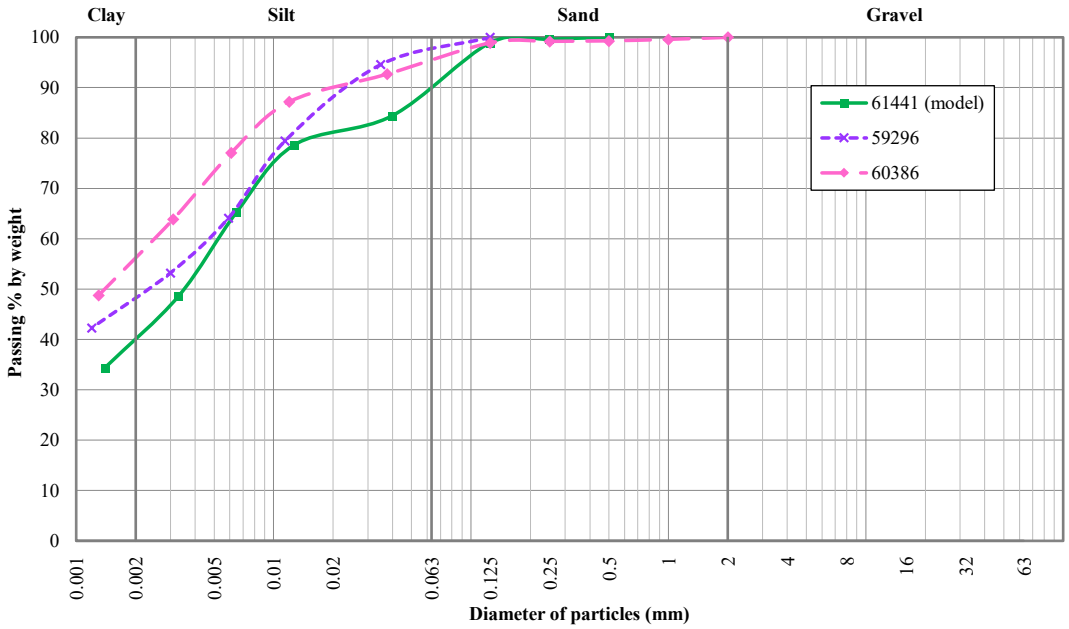

Fig. 4.3 Particle size distribution curves of tested materials.

Table 4.1 Index properties of tested materials.

Sample	Plastic Limit w_P (%)	Liquid Limit w_L (%)	Plasticity Index I_p (%)	Particle Density ρ_s (g/cm^3)	Natural Water Content w_n (%)
59296	37.2	55.2	18	2.942	24.7
60386	23.9	53.8	29.9	2.627	19.5
61441	38.4	61.1	22.7	2.731	-

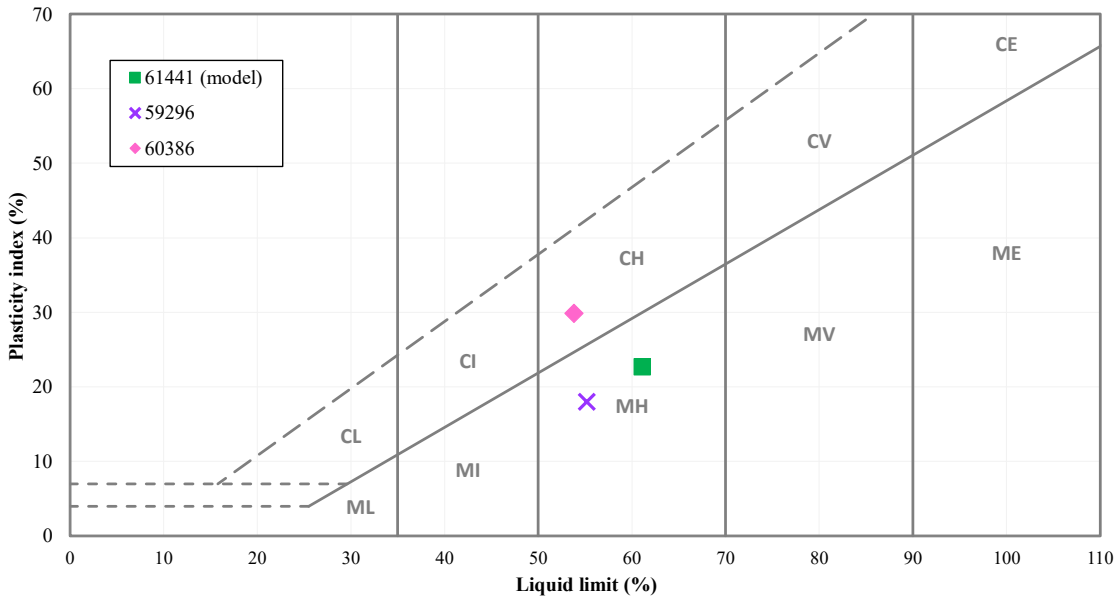

Fig. 4.4 Plasticity chart with positions of tested samples.

5. Physical Model

Physical models are a built-up version of an actual situation (a prototype). They can be bigger, smaller, or the same size as the prototype modeled. The enlarging model is created to concentrate on the prototype's behavior at a very small scale. The full-scale model is the most precise one but requires a lot of space, time, and money to create. To study a complex problem in a laboratory, we use the scaled-down model, which I will focus on in this thesis. Its advantage is the complete control over initial and boundary conditions. Furthermore, the short drainage paths result in faster consolidation and, therefore, in a shorter test duration.

A small-scale physical model of clay-fill (from now on 'the model'), tested in the large triaxial cell, is a crucial part of this thesis. It is made from a lumpy material sampled in the Bílina mine and scaled-down at a ratio of 1:20. A cylindrical sample with a height and a diameter of 15 cm corresponds to a dimension of 3 m at the full scale. Two models were created for greater confidence of the obtained results. Both models were prepared and tested similarly (except for the difference discussed in Chapter 5.3.1).

The purpose of these models is to study structural changes under the gradually increased effective stress. Two parameters were used for the quantification of changes: isotropic compressibility and hydraulic conductivity. The isotropic compression is a compression of the soil induced by loading with equal all-round stress. The soil decreases its volume in all directions proportionally (see Fig. 5.1). When the soil is loaded isotropically, no shear stresses (strains, respectively) develop. Hydraulic conductivity is the ability of the soil to seep water through its pores.

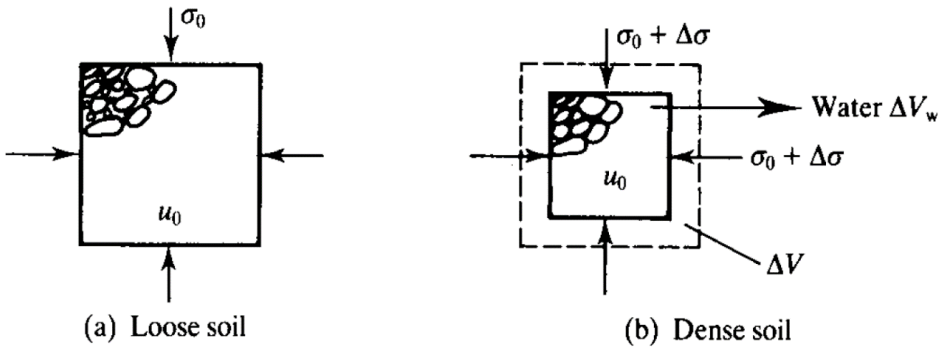

Fig. 5.1 Volume changes in soil under isotropic loading (Atkinson, 2007).

Accelerated changes of these parameters accompany changes in the structure. To separate the effects of the structure from the effects of the material behavior, series of

standard laboratory tests on reconstituted and undisturbed samples were carried out. Those tests are described in chapters 6 and 746.

5.1. Preparation of the model

The preparation of the models started by mixing the material. From the commercial laboratory SG Geotechnika a.s., the dried material (discussed in chapter 4) was received from the commercial laboratory SG Geotechnika a.s.; the material was divided into several fractions (in millimeters): 22.4 – 31.5, 16 – 22.4, 8 – 16, 4 – 8, 2 – 4, 1 – 2, 0.5 – 1, 0.25 – 0.5 and 0 – 0.25. The dry material was used to prevent the lump contact bonding during model preparation, which would result in higher porosity (see Fig. 2.5). Knowing the particle size distribution curve of the fresh fill and its twenty times smaller equivalent, the appropriate percentage of every fraction was calculated to fit the scaled-down curve (Fig. 5.2). The soil was not completely dry as it sucked in some hygroscopic water from the air during the manipulation. Each fraction's water content was determined with results ranging from 2.47 to 3.13 %, and their dry mass defined. According to the calculated distribution curve for the model, the fractions of corresponding weight were mixed (see Fig. 5.3). For the construction of two identical models, the homogenized mixture was split into even halves. To estimate the amount of mixture needed for filling the specimen form, its unit weight γ was determined at 13.3 kN/m^3.

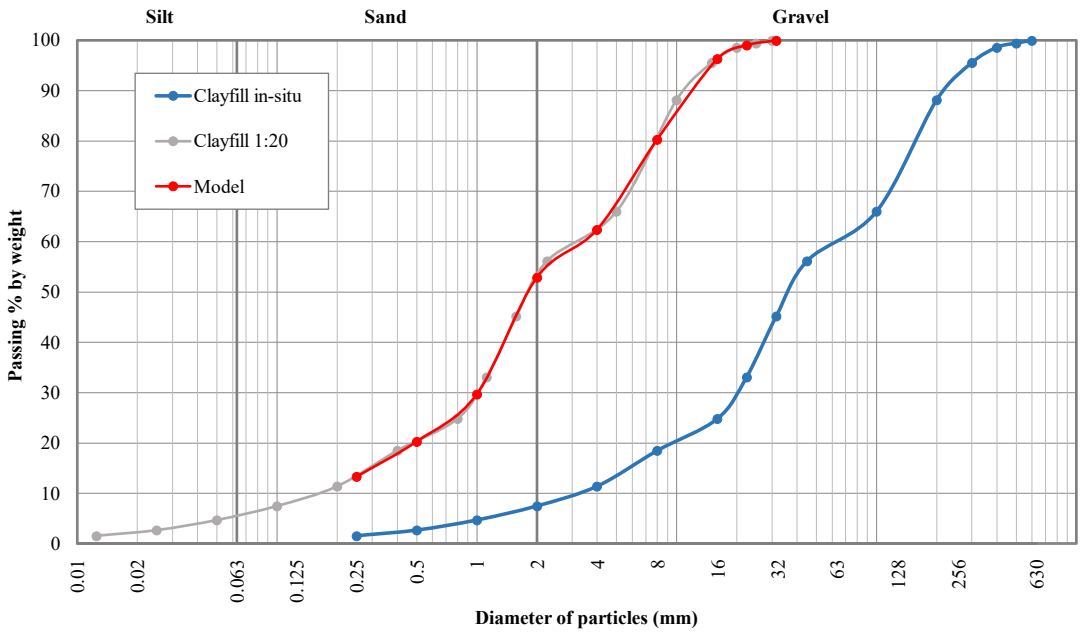

Fig. 5.2 Particle size distribution curves of clay fill in-situ, clay fill scaled-down twenty times, and the model mixture.

Fig. 5.3 Model mixture before testing.

To prevent the rubber membrane damage, all the sharp edges (including the edges of porous disks) were taped. Two rubber membranes were used to prevent leakage if one of them is damaged. The porous disks, filter papers, and all drainage paths were dry.

The mixture was poured extremely slowly and carefully into the form sitting on the base pedestal, simulating the in-situ filling, while trying to create the sample as homogenous as possible (Fig. 5.4a). Furthermore, the top of the sample was gently flattened and covered with filter paper, a porous disk, and the top cap. Next, the membranes were fixed to the top cap using the O-rings, and the supporting form was removed (Fig. 5.4b), and the cell was filled with water.

Fig. 5.4 Model 2 preparation. (a) Sample poured into the brown form. (b) Sample ready for testing.

5.2. Saturation

Before the saturation, the bottom base drainage line was flooded and connected to a funnel. The funnel filled with distilled water was adjusted to a stand allowing the funnel to move in the vertical direction and covered with a plastic foil so the water could not evaporate (see the saturation setup in Fig. 5.5).

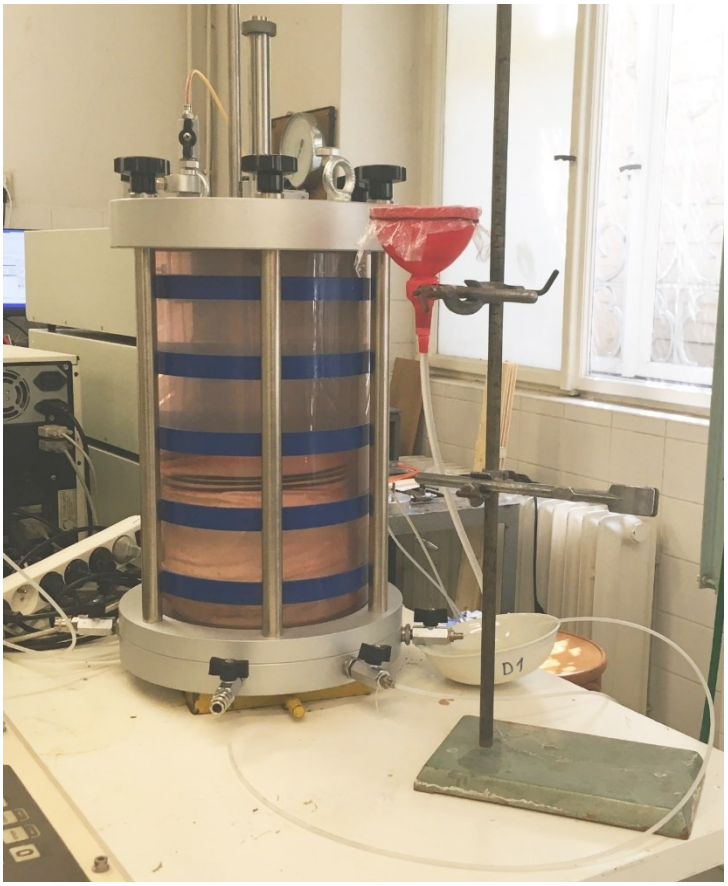

Fig. 5.5 Saturation of the model. Red funnel containing the distilled water connected to the bottom base of the large triaxial cell.

With the water level right under the bottom porous disk, the saturation started by a gradual rising of the funnel's level. After 1.5 to 2 months, the top of the sample was reached. Connected to a pressure controller, the cell was pressurized to 30 kPa (the first model) and 10 kPa, respectively (the second model). Water was slowly dripping from the valve.

After further two months of saturation, only water remained with no air bubbles coming out of the sample for a long time. The sample was assumed to be saturated and the testing started. Due to the extremely soft structure of the model, no direct verification of the saturation (e.g., B-check typical for triaxial tests) was done.

5.3. Test procedure

On the model, isotropic compressibility and hydraulic conductivity were tested in several loading stages (25, 50, 100, 200, 400, and 800 kPa). Every following effective stress increment is twice the previous one to preserve the constant effective stress and volume change steps in a resulting semi-logarithmic chart. First, the sample was compressed by a given load, and its consolidation was observed. Then, the corresponding hydraulic conductivity was measured. Table 5.1 and Table 5.2 list the applied pressures during the testing.

Table 5.1 Pressures applied to models during the compressibility testing (cell pressure (C), pressure at the bottom base (BB), and pressure at the top base (TB)). All pressures are given in kPa.

	MODEL 1			MODEL 2		
Loading stage	C	BB	TB	C	BB	TB
25	-	-	-	40	15	15
50	50	0	0	65	15	15
100	100	0	0	115	15	15
200	200	0	0	215	15	15
400	410	10	10	415	15	15
600	610	10	10	-	-	-
800	810	10	10	815	15	15

Table 5.2 Pressures applied to models during the hydraulic conductivity testing (cell pressure (C), pressure at the bottom base (BB), pressure at the top base (TB), pressure difference (Δu), and hydraulic gradient (i)). All pressures are given in kPa.

	MODEL 1					MODEL 2				
Loading stage	C	BB	TB	*Δu*	*i*	C	BB	TB	*Δu*	*i*
25	-	-	-	-	-	40	25	15	10	7.5
50	50	9.2	0.7	8.5	6.7	65	25	15	10	7.6
100	100	9.1	0.8	8.3	6.9	115	25	15	10	7.8
200	200	30	0	30	24.7	215	35	15	20	15.7
400	410	40	10	30	25.1	415	65	15	50	40.1
600	610	70	10	60	50.8	-	-	-	-	-
800	810	110	10	100	85.4	815	115	15	100	82.4

During the testing, a small amount of air was going out of the sample in bubbles. Despite the very long saturation, probably not all the lumps had fully saturated. Some air bubbles might remain inside the largest lumps, as the water flowed primarily through the

preferential paths in macrovoids and not through the lumps. The air was released within the testing by the pressure rise.

5.3.1. Isotropic compression

At every loading stage, a particular procedure was followed. First, sample valves were closed, and the cell was pressurized to a required pressure. Then, data logging was started, and simultaneously both sample valves were opened. During the ongoing test, the resulting consolidation curve was checked regularly to see if the excess pore pressures had already dissipated. Finally, when the consolidation was assumed to be finished, the hydraulic conductivity testing started.

The consolidation curves of model 1 at 100 and 200 kPa did not seem to be stabilizing (Fig. 5.6), probably due to leakage of the system. After the loading stage at 200 kPa, the test was interrupted, and the model was fully unloaded. The effect of the clay fill model's unloading at the low loading pressures is, according to Najser (2010), negligible, so it is expected that the unloading-reloading cycle did not significantly affect the test. It was found that the leakage was caused by malfunctioning O-rings. The cell was tested with two new O-rings added (six in total), and the model was reconsolidated to 200 kPa. When the sample's volume stabilized, the testing continued following the regular procedure.

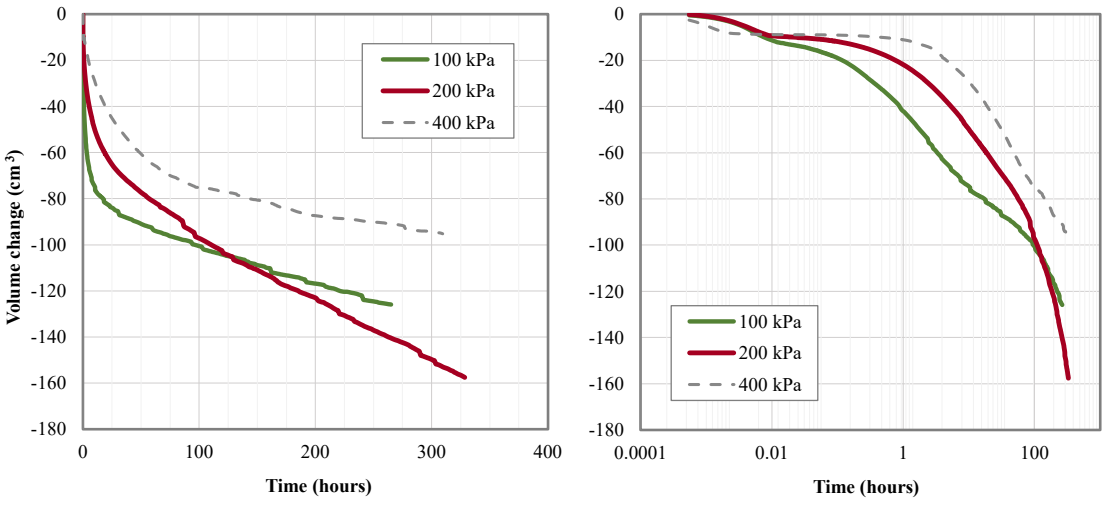

Fig. 5.6 Leakage, during the consolidation of model 1. The gray dashed line of the 400 kPa loading stage is representing a typical behavior. The green line is showing an increased volume change, already at 100 kPa. The red line displays an accelerated volume change and no stabilization during the loading at 200 kPa.

At the high pressures of model 2 testing (especially at 800 kPa), similar behavior was observed (see Fig. 5.10).

5.3.2. Hydraulic conductivity

A hydraulic conductivity test followed every consolidation stage. Hydraulic gradient (pressure difference between the top and bottom base over the drainage path's length) appropriate to the consolidation level was created. Pressure difference generates a flow of water going from the higher pressure end (bottom of the sample) to the lower pressure end (sample top). Values of pressure differences Δu between the bottom and top bases are listed in Table 5.1.

For hydraulic conductivity testing, the following procedure was applied. After the consolidation stage, the bottom base pressure controller was set to the required pressure. Several days later, when the flow stabilized, the pressure returned to its original value. After a few hours needed for the flow to stop, the bottom part of the sample, which was under the lower effective stress, reconsolidated. The next loading stage continued afterward.

5.4. Completion of test and postmortem analysis

When the last measurement was finished (hydraulic conductivity at 800 kPa), the sample was unloaded. After eight days, the volume change of the sample stabilized, so the cell could be dismantled, and the sample removed. To see the changed structure, the sample was divided into halves by pressing it between two desks in the loading frame (Fig. 5.7). The water content of five relic lumps and five samples representing the matrix separated was measured. Besides, the volume of the lumps under the water was measured as well. According to the procedure presented in (ASTM, 2003), three lumps were used for suction measurement using filter paper. The lumps were cut in halves, two regular filter papers covering the standardized filter paper were inserted in between, and the water content was subjected to equilibration for a week. The suction was calculated using the given parameters of the standardized filter paper and its water content.

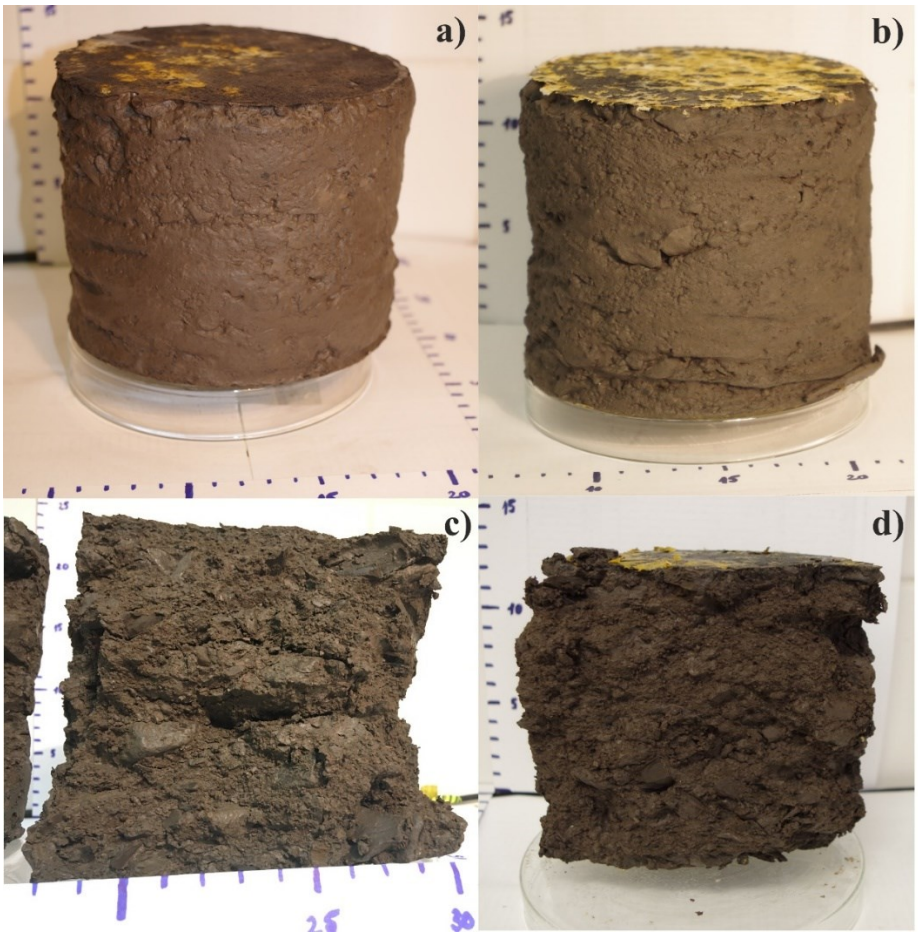

Fig. 5.7 Model 1 (left) and model 2 (right) after the test, before (top) and after (bottom) splitting into halves.

5.5. Data processing

For water content w (%) calculation, the following equation was used:

$$w = \frac{m_w}{m_d} \tag{3}$$

where m_w (g) is the mass of water and m_d (g) is the dry mass of soil. The volume V (cm^3) is determined from weighing under the water, where 1 gram of displaced water equals 1 cm^3 of the sample's volume, and from dimensions measured as a confirmation.

5.5.1. Isotropic compression

The critical parameter of compressibility is the void ratio e (-). It is defined as:

$$e = \frac{V_p}{V_s} \tag{4}$$

where V_p the volume of pores, and V_s the volume of soil grains, are calculated as:

$$V_s = \frac{m_d}{\rho_s} \tag{5}$$

and:

$$V_p = V_t - V_s \tag{6}$$

Particle density ρ_s is given in chapter 4.

The void ratio was calculated at the end of every loading stage. The volume measured under the water at the end was used as a reference value. Finally, the obtained void ratios were plotted against the logarithm of mean effective stress *p'* to get the resulting compression line (discussed in chapter 5.6.1).

Another parameter of interest was the coefficient of consolidation c_v (m^2/year). This parameter corresponds to one-dimensional (oedometric) compression. In the case of isotropic compression, we talk about the coefficient of consolidation for isotropic consolidation c_{vi} (m^2/year). C_{vi} does not equal c_v. However, Rowe's (1959) multiplying factor enables derivation from one to another. The factor that Head (1998) named f_{cv} is defined as:

$$f_{cv} = \frac{1}{1 - B(1 - A)(1 - K_0)} \tag{7}$$

where K_0 is the coefficient of earth pressure at the rest, and *A* and *B* are the Skempton's (1954) pore pressure coefficients. K_0 can be obtained from the Jáky's equation (Jáky, 1948):

$$K_0 = 1 - sin\,\varphi'_{cr} \tag{8}$$

where φ'_{cr} (°) is the critical state angle of friction which was gained from the triaxial test described in chapter 8. Coefficient *A* is an experimentally determined value varying by a clay type. With the knowledge of possible ranges of values presented by Skempton (1954), *A* was estimated to be 0.6. Coefficient *B* represents the degree of saturation. The model was presumed to be fully saturated; therefore, coefficient *B* equals 1. The resulting converting equation is thus given by:

$$c_v = f_{cv} * c_{vi} \tag{9}$$

To calculate c_{vi}, the log-time graphical method (also known as the Casagrande method) is used. It is a curve-fitting procedure, which compares the laboratory consolidation curve with the theoretical one. The goal is to delimit the primary consolidation phase and determine the time corresponding to its 50 %, t_{50} (min)(Fig. 5.8). This was carried out for each loading increment from the charts representing the change

of volume (y-axis in mm^3) in the logarithm of time (x-axis in minutes). The detailed procedure is described in Head (1994).

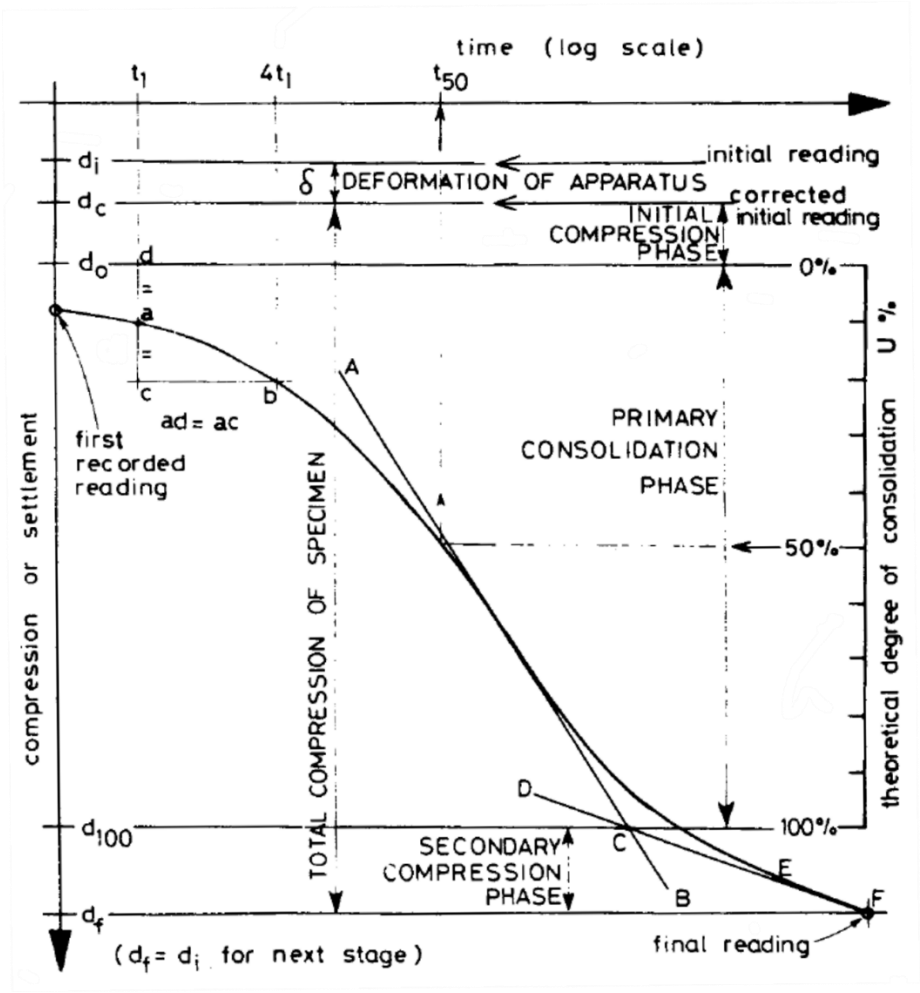

Fig. 5.8 Graphical analysis of a log-time/settlement curve (Head, 1994).

The time corresponding to 50 % of primary consolidation t_{50} (min) was used to calculate c_{vi}:

$$c_{vi} = \frac{T_{50} * H^2}{t_{50}} \tag{10}$$

where T_{50} (-) is the time factor and H (mm) the height of the sample. In the case of isotropic consolidation, the time factor equals 0.199 (Head, 1998). The height of the sample was calculated from the sample's total volume at t_{50} and its height/diameter ratio.

As the shape of the model's consolidation curves was, due to the double porosity, atypical, c_v was also calculated from the equation of the hydraulic conductivity given by Head (1998):

$$k = c_v * m_v * 0.31 * 10^{-9} \tag{11}$$

where k at the end of every loading stage is known (calculation described in the next chapter). It was necessary to calculate the coefficient of volume compressibility for oedometric consolidation m_v (m^2/MN). Its isotropic equivalent m_{vi} can be defined as:

$$m_{vi} = \frac{\delta e}{\delta p'} * \frac{1000}{1 + e_1} \tag{12}$$

where δe is the change in void ratio during the loading stage, $\delta p'$ is the effective stress increment, and e_1 is the void ratio at the beginning of the loading stage (Head, 1998). Head (1998) also presents the approximate relationship between m_v and m_{vi}:

$$m_{vi} = 1.5 m_v \tag{13}$$

5.5.2. Hydraulic conductivity

Based on Darcy's law, the hydraulic conductivity k (m/s) is a mean discharge velocity of flow of water in soil v (m/s) controlled by the hydraulic gradient i (-) (Head, 1994):

$$k = \frac{v}{i} \tag{14}$$

The discharge velocity v is defined as the rate of flow Q (ml/s) of water flowing through the cross-sectional area A (mm^2) of the sample:

$$v = \frac{Q}{A} \tag{15}$$

The rate of flow Q was calculated as a volume change at the top base ΔV during the stabilized flow over its duration t (s):

$$Q = \frac{\Delta V}{t} \tag{16}$$

The hydraulic gradient i (-) is a pore pressure difference Δu over the length of drainage path (the height of sample) L (mm):

$$i = \frac{\Delta u}{L} \tag{17}$$

To calculate the height of sample L and the area A, the sample's volume at the end of the consolidation stage and the height-diameter ratio (height over diameter, both measured during the completion of the test) were used.

The final form of the equation of coefficient of consolidation used is:

$$k = \frac{Q}{(A * i)} \tag{18}$$

5.6. Test results

5.6.1. Isotropic compression

The consolidation curves of all loading stages can be seen in Fig. 5.9 and Fig. 5.10. The volume changes are displayed against time both in linear (the left figure) and logarithmic (the right figure) scale. All the curves show that the volume change of models did not stabilize, even after a long loading period. In the second half of consolidation, the volume is changing linearly with time. It can be explained by the secondary compression (creep) caused by the squashing of ductile lumps. The mean volume change over the stage is approximately 100 cm^3. However, the volume changes at 100 and 200 kPa loading of model 1 and 800 kPa loading of model 2 are significantly higher. This is a result of the leakage discussed in chapter 5.3.1. The volume changes under 70 cm^3 were caused by smaller pressure increases (less than double the previous one).

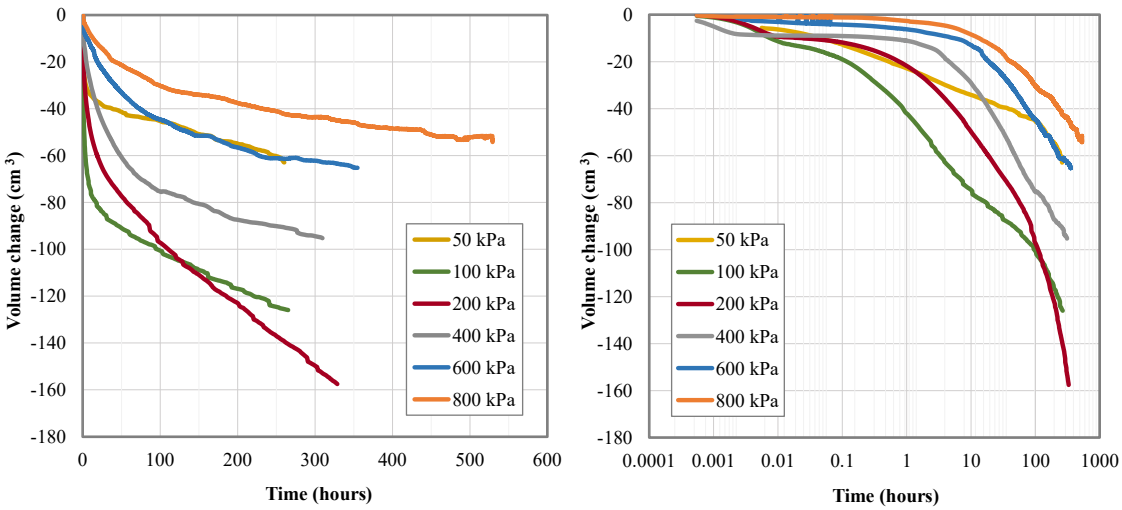

Fig. 5.9 Consolidation stages of model 1.

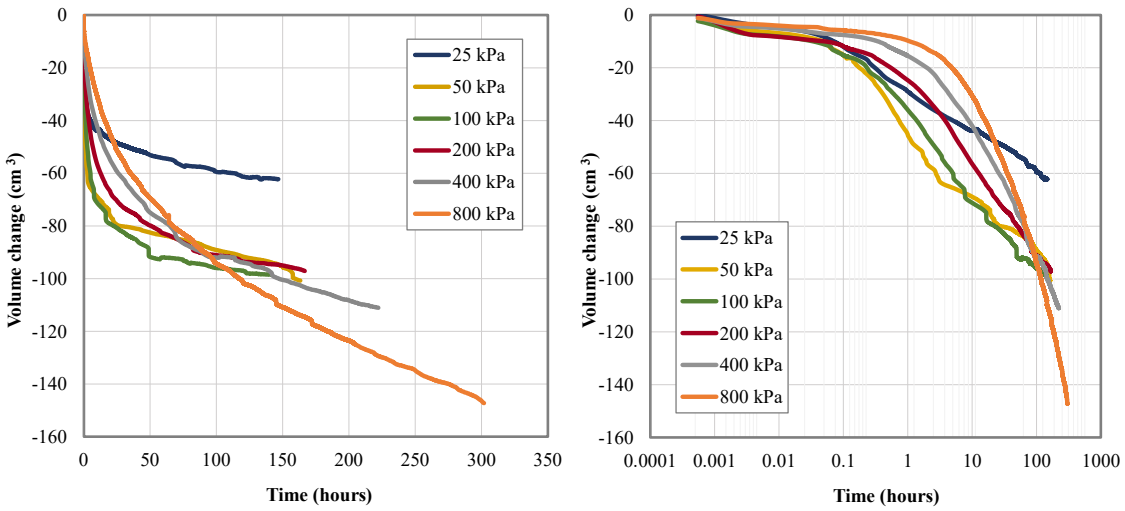

Fig. 5.10 Consolidation stages of model 2.

The resulting compression lines are shown in Fig. 5.11. Their mutual distance can be explained by a slight difference in initial void ratios developed during the models' preparations (despite the extremely careful preparation process) and the difference in duration of the loading stages of each model (discussed in chapter 9.4). The leaking can explain the difference between their slopes. However, in general, both compression lines are matching very well.

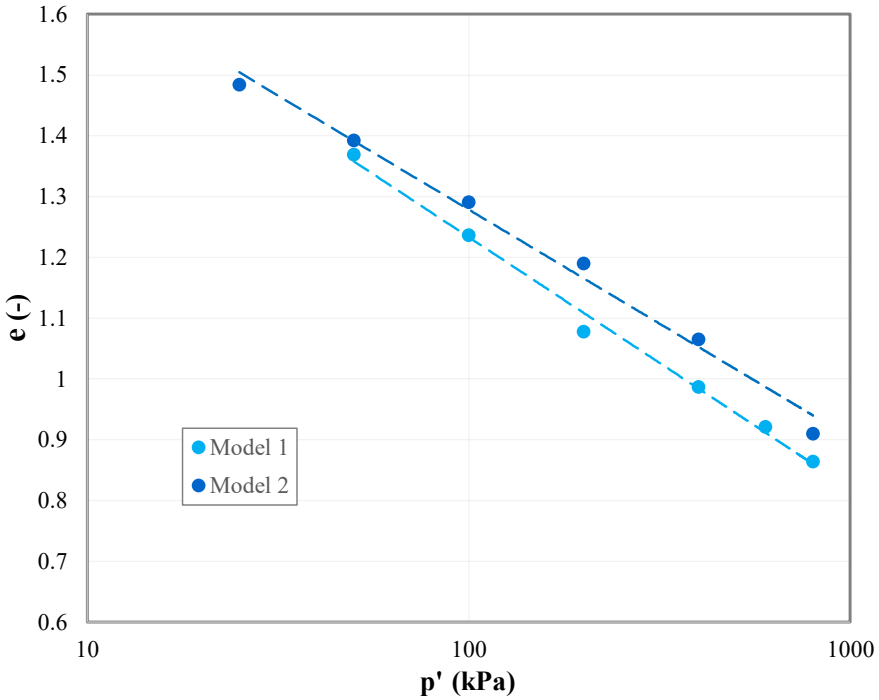

Fig. 5.11 Compression lines of models.

To assess the effect of leakage mentioned above, the volume changes over the three stages where the leakage was observed were replaced by the mean volume change of 100 cm^3. The resulting corrected compression lines are displayed with the original ones in Fig. 5.12. After the corrections, the lines are parallel and closer to each other. Also, the slopes slightly changed when comparing with the original ones. Nevertheless, the overall differences are relatively small; therefore, the original data are credible and were used for further analysis.

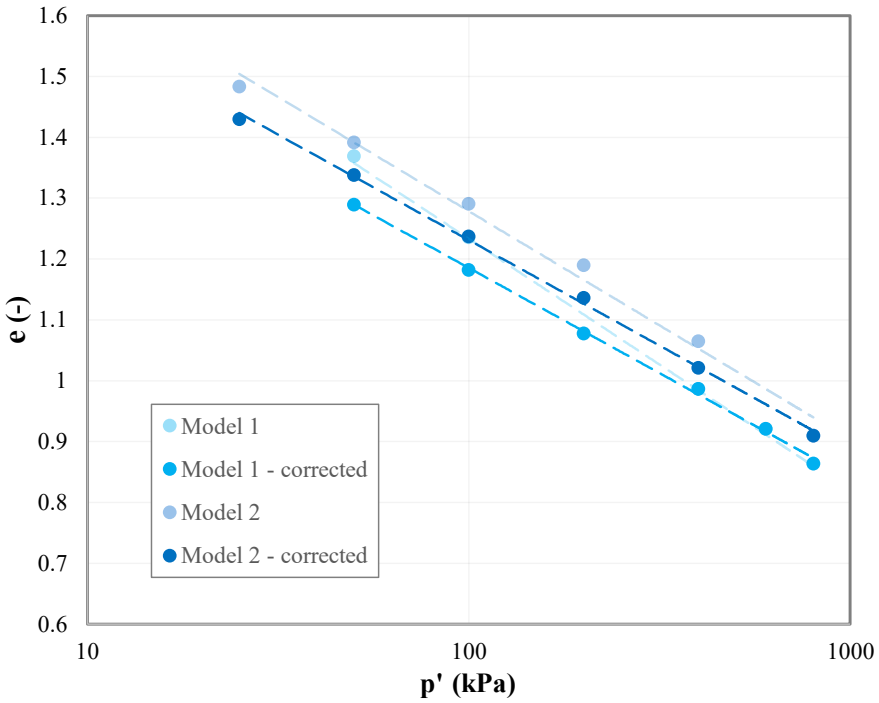

Fig. 5.12 Corrected compression lines of models.

Results of the parameter c_v are listed in Table 5.3. The models' consolidation curves used for the determination have a specific shape (see right charts in Fig. 5.9 and Fig. 5.10) caused by the double porosity. Therefore, their comparison with the theoretical consolidation curve (Fig. 5.8), which is the principle of the log-time method, was very complicated. It was possible to determine c_v only from the half of curves. However, the results are out of the expected range and do not support the observations made on compression lines. On the other hand, c_v values calculated from hydraulic conductivity have a reasonable range and confirm the higher porosity of model 2 seen above.

Table 5.3 Comparison of coefficient of consolidation of models calculated using the hydraulic conductivity and log-time method.

	MODEL 1		MODEL 2	
Loading stage (kPa)	c_v (m^2/year) from k	c_v (m^2/year) from log-time method	c_v (m^2/year) from k	c_v (m^2/year) from log-time method
25	-	-	34.919	-
50	3.950	-	7.560	148.140
100	1.219	65.274	2.903	40.811
200	0.435	-	2.102	13.284
400	0.622	26.590	1.176	-
600	0.319	13.709	-	-
800	0.328	-	0.971	-

5.6.2. Hydraulic conductivity

Fig. 5.13 and Fig. 5.14 present the dependence of flow on time for individual effective stresses. In the left charts, there are volume changes over time at all loading stages. The right chart describes 100 kPa and higher loading stages, where the hydraulic conductivity is significantly lower. The positive values of volume change represent the water going into the sample at its bottom, and the negative values, the water going out of the sample at its top.

The curves look very symmetrical. They indicate that the amount of water going in the sample is the same as the amount going out. At low pressure, the volume of water flowing through is large; therefore, the curves' fluctuations caused by the structural inhomogeneity are not significant. With increasing stress, the curves' fluctuations become more significant due to the decrease of the volume of water flowing through the sample (right charts). Taking the complex structure into account, the flow trend is not expected to be as linear as in the homogenous sample. Nevertheless, considering that hydraulic conductivity changes by several orders of magnitude throughout the testing, the inaccuracies are negligible.

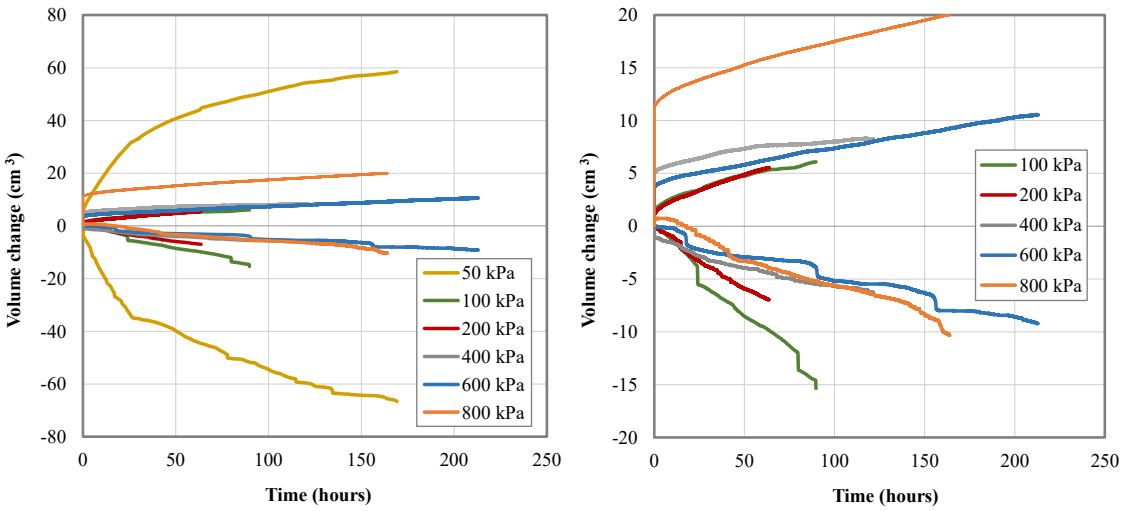

Fig. 5.13 Hydraulic conductivity measurements of model 1.

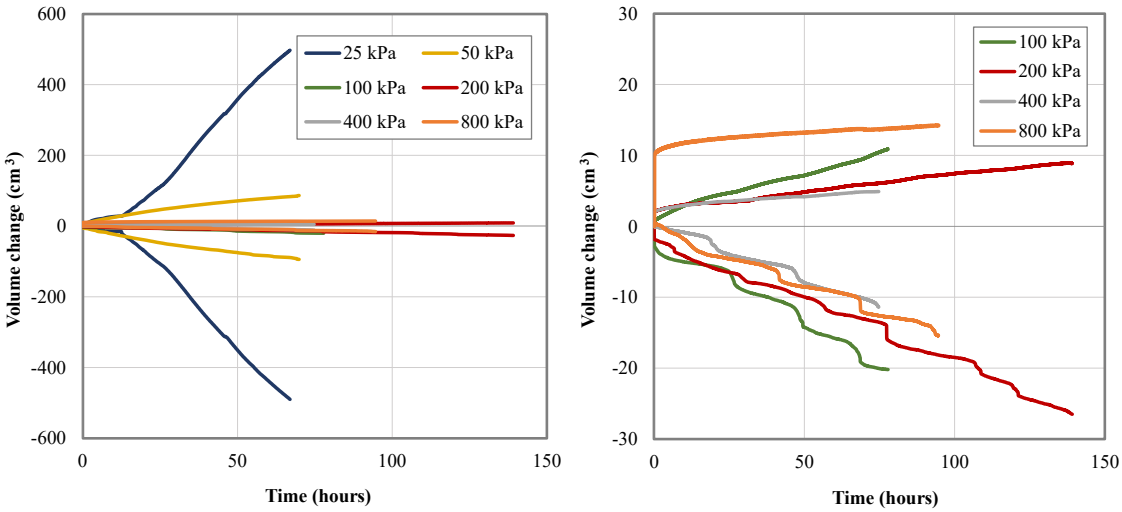

Fig. 5.14 Hydraulic conductivity measurements of model 2.

The resulting hydraulic conductivities are plotted in Fig. 5.15 against the mean effective stress on a logarithmic scale. Power trendlines demonstrate their trends. The tendencies are identical. However, the hydraulic conductivity of model 2 is higher, which corresponds with its higher void ratio displayed in Fig. 5.11.

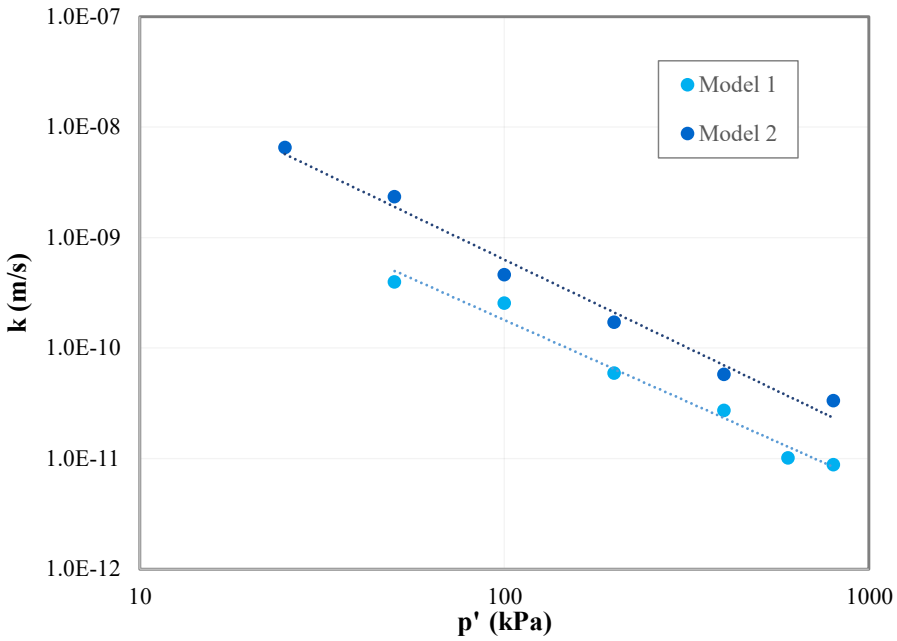

Fig. 5.15 Hydraulic conductivity of models.

5.6.3. Postmortem analysis

Table 5.4 lists the results of measurements made after the testing. It shows the total water content of the model, mean water contents of lumps and matrix, and the lumps suction. Lower suction values of model's 1 lumps correspond to their higher water content. The lower water content of the model 2 lumps might result from the incomplete saturation as the testing time was shorter than for model 1. However, the differences in water content are minimal, which implies the preferential path closure and relative homogenization of the model at the end of testing.

Table 5.4 Results of postmortem analysis.

	MODEL 1			MODEL 2		
Total *w* (%)	33.1			32.3		
Lumps *w* (%)	32.1			30.0		
Matrix *w* (%)	32.1			31.3		
Lump's suction (kPa)	125	82	101	141	126	135

6. Isotropic compressibility and hydraulic conductivity

For correct interpretation of the model's results, the knowledge of the possible structural behavior range is necessary. Therefore, a series of isotropic compression and oedometric tests were carried out to characterize the behavior of reconstituted and undisturbed material necessary for the description of the model's structural transition. This chapter describes the tests made on reconstituted samples to find the parameters of the material with no structure. Those should represent the state of an entirely degraded fill. Samples 59296, 60386, and 61441 (the model material), described in chapter 4, were subjected to testing.

6.1. Sample preparation and test procedure

At first, a slurry of water content higher than the liquid limit was created. For sample 61441, the lump fraction 2-4 mm was used. In the case of samples 59296 and 60386, the drill core trimmings from the preparation of undisturbed oedometers (chapter 7.1) were utilized.

The preconsolidated sample was prepared from the slurry. The consolidometer of 38 mm in diameter was used to preconsolidate the sample up to 50 kPa. The slurry was carefully poured into the consolidometer so that no air bubbles were trapped in there. The consolidometer was set in the room with constant temperature and a loading frame was put on it (Fig. 6.1 a). The sample was loaded stepwise up to 50 kPa. It was kept saturated for the entire consolidation process, which took a minimum of 5 weeks.

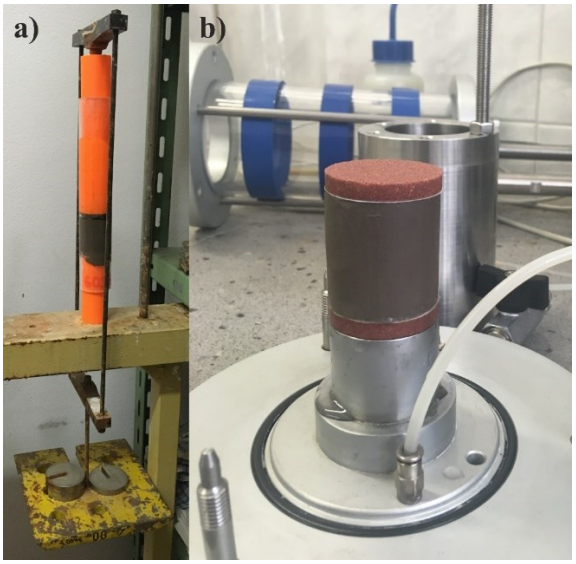

Fig. 6.1 Preparation of reconstituted sample 60386 for isotropic compression.

Before the test, the porous disks were saturated (for 24 hours), the cell was checked, and the drainage lines flooded. Then, the preconsolidated sample was pushed out of the consolidometer, placed into a sample box, and cut to a required dimension. The width to diameter ratio 1:1 was used. Hence, the sample was cut to a height of 38 mm. The sample was weighed and its dimensions measured.

On the cell's base pedestal, the sample with filter papers and saturated porous disks at its bottom and top was placed (Fig. 6.1 b), while the top cap with the drainage line was emplaced on the top at last. Over the sample, the rubber membrane was placed using the membrane stretcher with applied suction. It was sealed with four O-rings (two at the bottom and two at the top). At last, the cell was fixed and filled with distilled water.

The test procedure was very similar to the model's one. I followed the loading steps at 25, 50, 100, 200, 400, and 800 kPa, and measured the isotropic consolidation and hydraulic conductivity.

First, the pressure controllers connected to the top and bottom base were set to 10 kPa and the cell pressure controller to 20 kPa. Then, the pressures were slowly raised by 290 kPa (sample 300 kPa and cell 310 kPa) at a 2 kPa/min rate. The effective pressure stayed at 10 kPa. After three days, when volume changes stabilized, the testing procedure started by the consolidation. The pressures applied during the testing are listed in Table 6.1 and Table 6.2.

Table 6.1 Applied pressures during the compressibility testing (cell pressure (C), pressure at the bottom base (BB), and pressure at the top base (TB)). All pressures are given in kPa.

	59296		60386		61441	
Load. stage	C	BB/TB	C	BB/BT	C	BB/BT
25	325	300	325	300	325	300
50	350	300	350	300	75	25
100	400	300	400	300	125	25
200	500	300	500	300	225	25
400	700	300	700	300	425	25
800	1100	300	1100	300	825	25

Table 6.2 Applied pressures during the hydraulic conductivity testing (pressure at the bottom base (BB), pressure difference (Δu), and hydraulic gradient (i)). Cell pressures and pressures at the top base are the same as for compressibility testing. All pressures are given in kPa.

	59296			60386			61441		
Load. stage	BB	*Δu*	*i*	BB	*Δu*	*i*	BB	*Δu*	*i*
25	309	8.7	22.7	308	8.4	21.9	308	8.1	20.4
50	308	8.3	21.9	308	8.4	22.1	33	8.3	21.1
100	309	8.5	22.9	309	8.8	23.5	33	8.2	21.3
200	309	9	24.9	309	8.9	24.2	34	8.5	22.5
400	319	19	54	319	19	51	44	19	51
800	350	50	144	349	49	137	74	49	136

Practically, the same testing procedure was followed as in the case of models (chapter 5.3). With the sample's valves closed, I pressurized the cell to the required pressure, opened the valves, and let the volume change to stabilize (approximately 2 days). Then, the hydraulic conductivity measurement started by increasing the pressure at the bottom base by a required value of *Δu*. After 2 to 3 days, the pressure was dropped back to 300 kPa, and one hour was needed for the flow to stop and the sample to reconsolidate.

After the last hydraulic conductivity measurement, the sample was fully unloaded. After 10 days, the cell was dismantled, and the sample removed and quickly weighed. Moreover, its dimensions and its volume under the water were measured (Fig. 6.2). The void ratio at every loading stage was calculated from these values and volume changes during the test. To process the data, the methods described in chapter 5.5 were used.

Fig. 6.2 Volume measurement of reconstituted sample 61441 under the water after the isotropic compressibility test.

6.2. Test results

The results are presented in an analogous form to the models' results. Fig. 6.3, Fig. 6.4, and Fig. 6.5 represent the consolidation curves at all loading stages of all three samples. Again, the volume changes are displayed against time in linear (the left figure) and logarithmic (the right figure) scale. All the curves show the stabilization reached after approximately 24 hours. Volume changes at loading stages 25 and 50 kPa are about a quarter (or a half, respectively) of the volume changes at the higher stages. This results from preconsolidation up to 50 kPa during the preparation process, and it affects the calculation of the coefficient of consolidation. The consolidation curves of sample 61441 (Fig. 6.5) have a smooth course. To the contrary, the consolidation curves of samples 59296 (Fig. 6.3) and 60386 (Fig. 6.4) register a fluctuation in measurements every 24 hours. These samples were tested in a different room than sample 61441. It is most likely that the fluctuations result from periodic exposure to sunlight. However, they did not affect the final volumes.

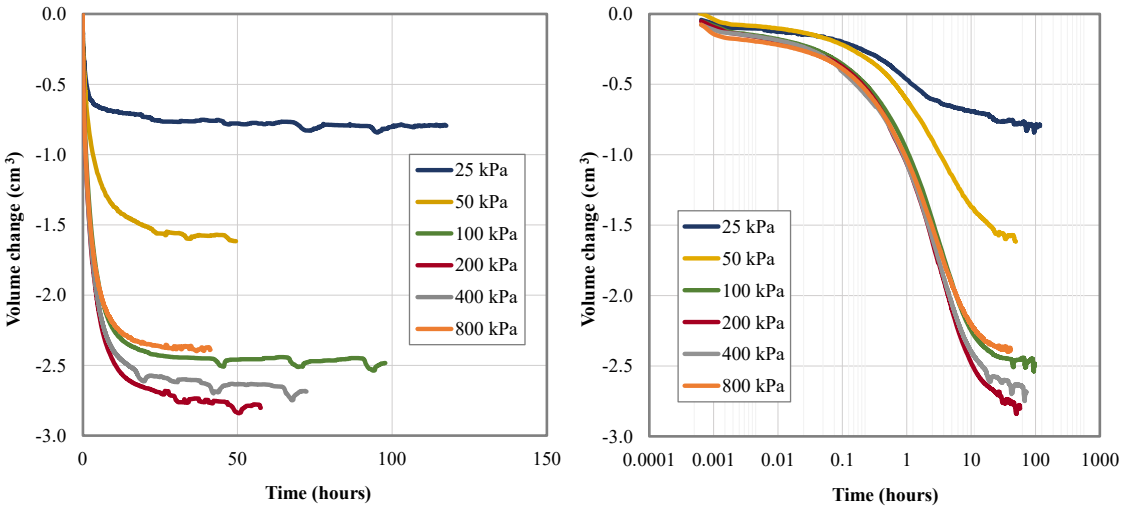

Fig. 6.3 Consolidation stages of isotropically consolidated reconstituted sample 59296.

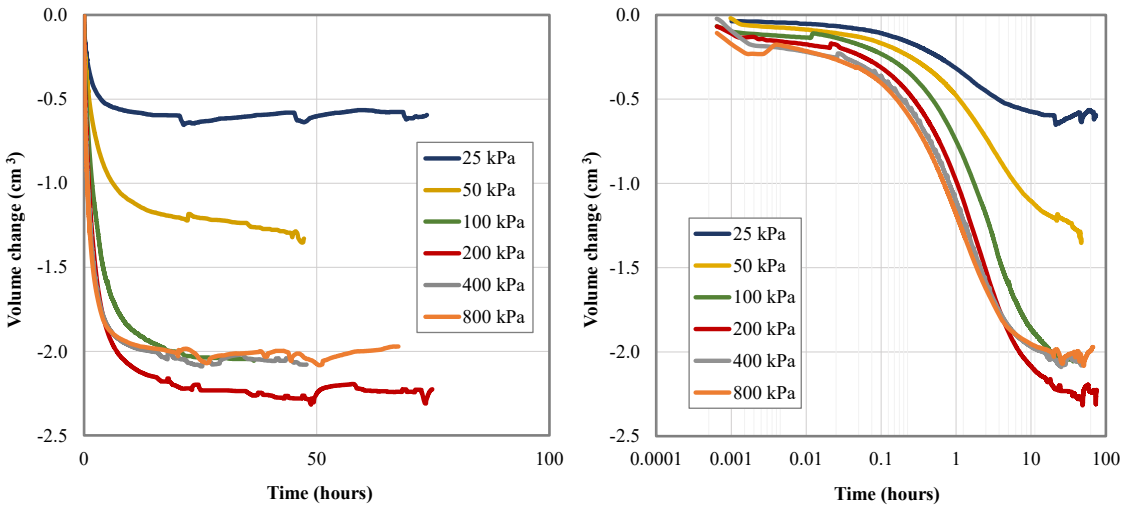

Fig. 6.4 Consolidation stages of isotropically consolidated reconstituted sample 60386.

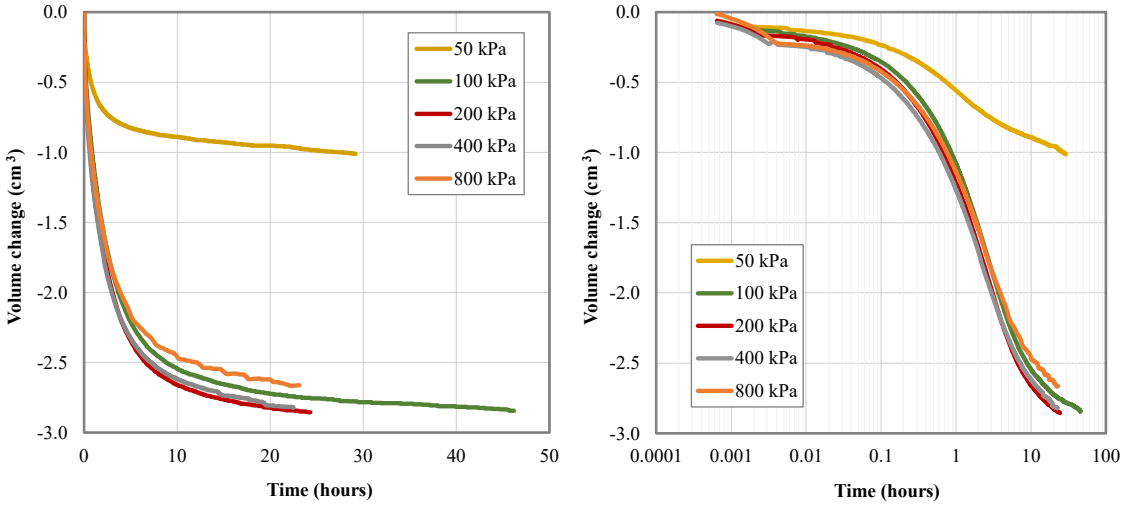

Fig. 6.5 Consolidation stages of isotropically consolidated reconstituted sample 61441.

Fig. 6.6 presents the compression lines of reconstituted samples; therefore, the normal compression lines (NCL) of all tested materials. Table 6.3 lists compression line parameters λ and N. λ is a gradient of the line, and N is the value of $(1+e)$ at $p' = 1$ kPa ($\ln p' = 0$). The model material (sample 61441) has the highest void ratio and the steepest line. Sample 59296 lies very close to the compression line of sample 61441 and has a similar gradient. However, sample 60386 shows a distinct character. Its gradient is almost half of the sample's 61441 gradient and N is smaller by 1.

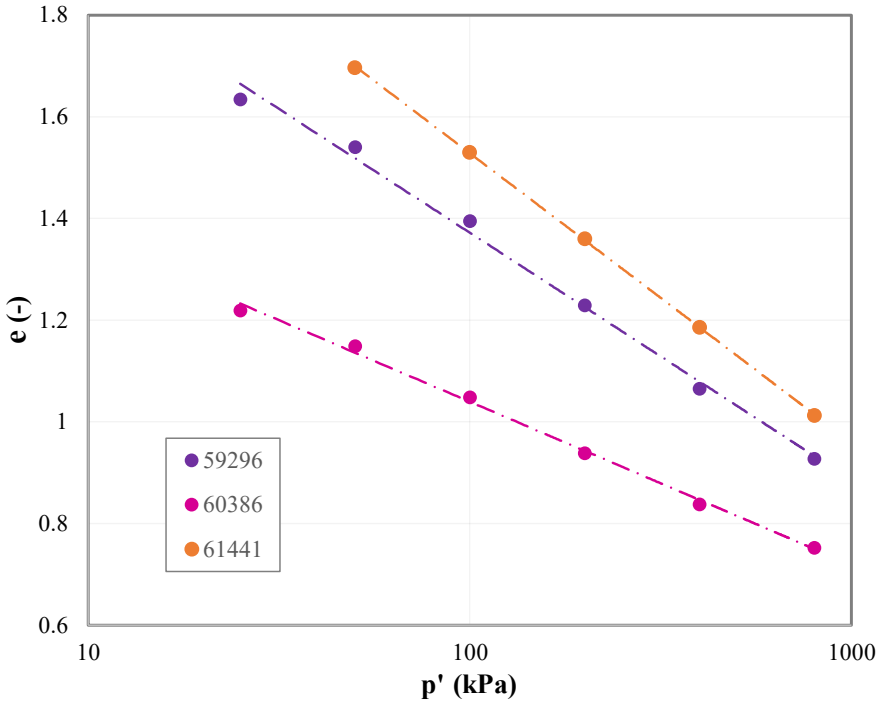

Fig. 6.6 Compression lines of isotropically consolidated reconstituted samples.

Table 6.3 Parameters of compression lines. λ is the gradient and N is the value of (1+e) at ln p' = 0.

	59296	60386	61441
λ	0.211	0.139	0.247
N	3.345	2.681	3.666

The coefficients of consolidation calculated by the log-time method are listed in Table 6.4. At 25 and 50 kPa stages of loading, the c_v values are higher than at the subsequent stages. The difference is caused by the preconsolidation discussed above.

Table 6.4 Coefficient of consolidation of isotropically consolidated reconstituted samples.

	59296	60386	61441
Loading stage (kPa)	c_v (m^2/year)	c_v (m^2/year)	c_v (m^2/year)
25	11.96	8.12	-
50	4.39	3.99	12.44
100	3.45	4.01	4.12
200	3.38	5.14	4.78
400	3.50	7.52	5.34
800	3.44	7.77	4.47

Hydraulic conductivity measurements of the samples are displayed in Fig. 6.7. The measurements show a linear trend and approximately equal amount of incoming and outcoming water.

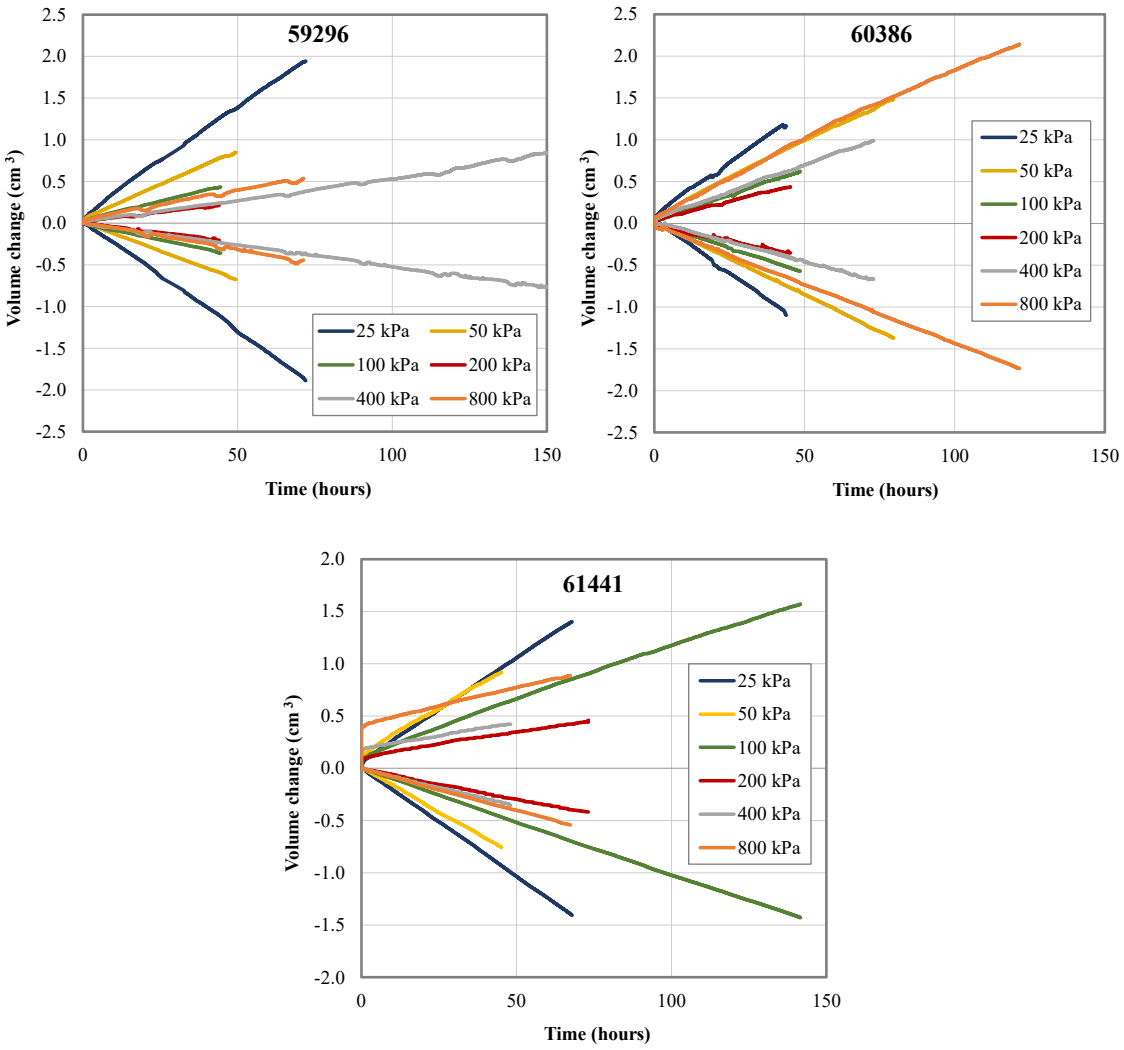

Fig. 6.7 Hydraulic conductivity measurements of isotropically consolidated reconstituted samples.

Hydraulic conductivities of the samples are displayed in Fig. 6.8. against the mean effective stress at a logarithmic scale. Power trendlines demonstrate their trends. All of them are of the same order of magnitude but slightly different slopes. However, the hydraulic conductivity of sample 60386 is the highest, which contradicts its lowest porosity mentioned above (Fig. 2.1).

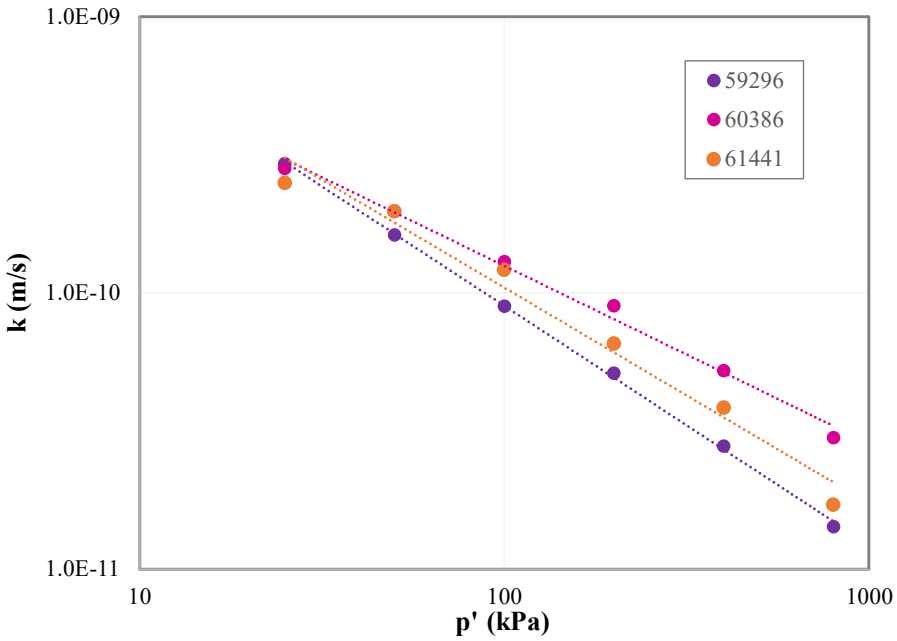

Fig. 6.8 Hydraulic conductivity of isotropically consolidated reconstituted samples.

7. One-dimensional compressibility

Another type of compressibility tested is the one-dimensional one. One-dimensional compression is a compression of soil induced by loading with axial stress. The deformation in other directions is precluded so that the soil deforms solely in the loading direction (the settlement). It simulates the conditions of soil under the earth pressure when horizontal movement is not possible due to the presence of the surrounding soil. The axial loading generates the vertical effective stresses σ_v' and shear forces (stresses, respectively) develop.

One-dimensional compression is tested in an oedometer consolidation cell. A rigid metal ring confines the sample's sides. At the bottom and top, porous disks are enabling drainage. The load (generated by the weight placed on a lever arm) is applied on the sample via the top cap in the loading stages. The units measured include only the settlement (height change Δh) by the dial gauge and the time. The sample is saturated throughout the test.

In oedometers, all the studied materials were tested in reconstituted (59296, 60386, and two times 61441) and undisturbed (59296 and 60386) states, as these allow the testing at higher loading than the isotropic compression in the triaxial cell.

7.1. Sample preparation

First, the undisturbed samples were prepared from the drill cores. I cut out the core's sides and, in its center, created a cylindrical pile at least 4 mm wider than the final sample diameter. The confining ring's inner dimensions are 5 cm in diameter and 2 cm in height. Pushing the ring of the known weight into a pile, the sides were trimmed simultaneously so that the sample could fit in (see Fig. 7.1). Finally, the top and bottom parts were cut and flattened. The sample was weighted with the ring and assembled in the consolidation cell with dry filter papers and porous disks (wet disks would cause swelling). After setting up the load frame, adjusting the beam, setting the dial gauge, and adding a small weight (0.5 kg) to a hanger, the settlement's recording started, and the sample was flooded. The sample started to swell, which was resolved by load increasing and keeping it at the zero vertical deformation. When reaching the load equal to the swelling pressure (59296 – 1150 kPa, 60386 – 300 kPa), the sample was subjected to stabilization for several days.

Fig. 7.1 Preparation of undisturbed sample 60386 from drill core.

From the trimmings (samples 59296 and 60386) and lumps (61441), I prepared the reconstituted samples (described in chapter 6.1). The confining metal ring, standing on the saturated bottom porous disk and the filter paper, was carefully filled with slurry so that no air bubbles were trapped. I flattened the top, assembled the consolidation cell, gently placed the filter paper and the top saturated porous disk on, quickly set up the loading frame, started the settlement recording, and flooded the sample. After the settlement's stabilization, a small weight was added to the hanger, and another cycle of stabilization started. This procedure was repeated until reaching 25 kPa loading stress applied on the sample. Then, the sample was quickly unloaded, the apparatus disassembled, the ring with the sample weighted, the sample's height measured, and the sample reassembled again. After reloading to 25 kPa, the testing procedure started.

7.2. Test procedure

The test plan consisted of three loading and unloading branches. The corresponding loading and unloading stages are listed in Table 7.1. They would be the same for all samples; however, in the case of the undisturbed samples, it was necessary to skip the loading stages below the swelling pressures and to add two loading stages for sample 59296. Every loading/unloading stage took approximately 24 hours.

Table 7.1 Loading and unloading stages at the reconstituted (R) and undisturbed (U) oedometer tests. Stresses are given in kPa.

59296 60386 R 61441	25	40	70	120	60	25	60	25	60	120 ▸
	▸ 200	400	200	100	50	25	50	100	200	400 ▸
	▸ 800	1600	2200	1600	800	400	200	100	50	25
59296 U	1150	1300	1600	1900	2200	1900	1600	1300	1150	
60386 U	300	400	300	400	800	1600	2200	1600	800	400 ▸
	▸ 300									

7.3. Completion of test

When the last unloading stage was finished, the sample was fully unloaded. Two days later, the sample was removed, weighted, and its height measured. These values were used for the verification of calculation of the void ratio.

7.4. Data processing

From the sample's height at the beginning of the test H_0 (mm) and the recorded cumulative settlement ΔH (mm), the sample's height at the end of every loading stage H (mm) was calculated as:

$$H = H_0 - \Delta H \tag{19}$$

During the oedometer test, the sample's diameter, therefore, its area A (mm^2), is constant. It was used to calculate the sample's total volumes V_t (mm^3):

$$V_t = H * A \tag{20}$$

Using the equations (4), (5), and (6) given in chapter 5.5.1, the void ratios e (-) were calculated.

To compare the oedometric and isotropic compression results, the mean effective stresses p' (kPa) corresponding to vertical effective stresses σ'_v (kPa) of each load step was determined as:

$$p' = \frac{1}{3}\sigma'_v * (1 + 2K_0) \tag{21}$$

where K_0 is the coefficient of earth pressure at the rest obtained from Jáky's equation (8) operating with the critical state angle of friction φ'_{cr} (°), hereafter discussed in chapter 8.

The oedometer consolidation cell I used does not enable direct hydraulic conductivity measurement. Nonetheless, the hydraulic conductivity can be calculated from c_v (m^2/year) and m_v (m^2/MN)(equations (11) and (12) where m_{vi} equals m_v). C_v is then calculated from equation (8), where c_{vi} equals c_v and the time factor T_{50} (-) equals 0.026 (Head, 1994). The time corresponding to 50 % of primary consolidation t_{50} (min) was determined according to the procedure described in Fig. 5.8, and the height H (mm) at time t_{50} from the settlement measurements.

7.5. Test results

Fig. 7.2 presents, as an example of the typical oedometer test course, all the consolidation stages of reconstituted sample 59296. Negative height changes represent the loading stages (L), and positive height changes the unloading stages (U). The three loading/unloading branches are numbered (1 - 3).

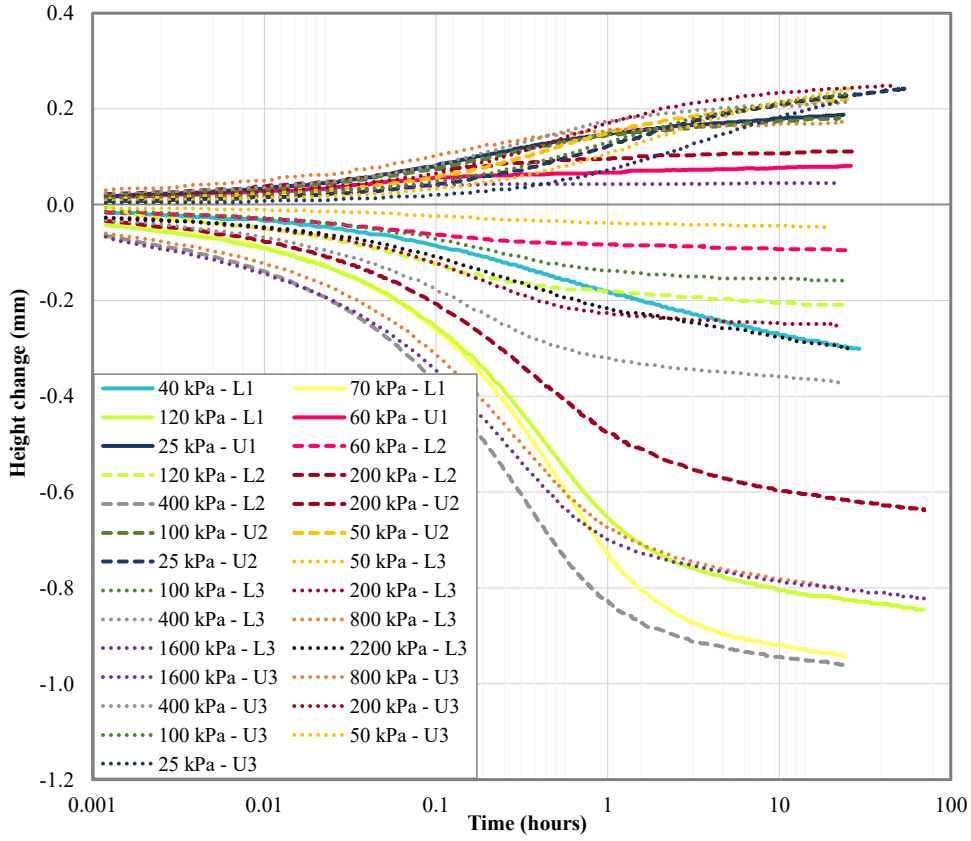

Fig. 7.2 All consolidation stages of sample 59296 on a semi-logarithmic scale.

The compression lines of the reconstituted samples 59296 and 61441 1 and 2, presented in Fig. 7.3, are practically identical. However, the line of the reconstituted sample 60386 lies significantly lower. The undisturbed compression lines lie significantly lower than their reconstituted equivalents. It is due to the preconsolidation of undisturbed samples, which results in a smaller initial void ratio and higher stiffness (gentler slope).

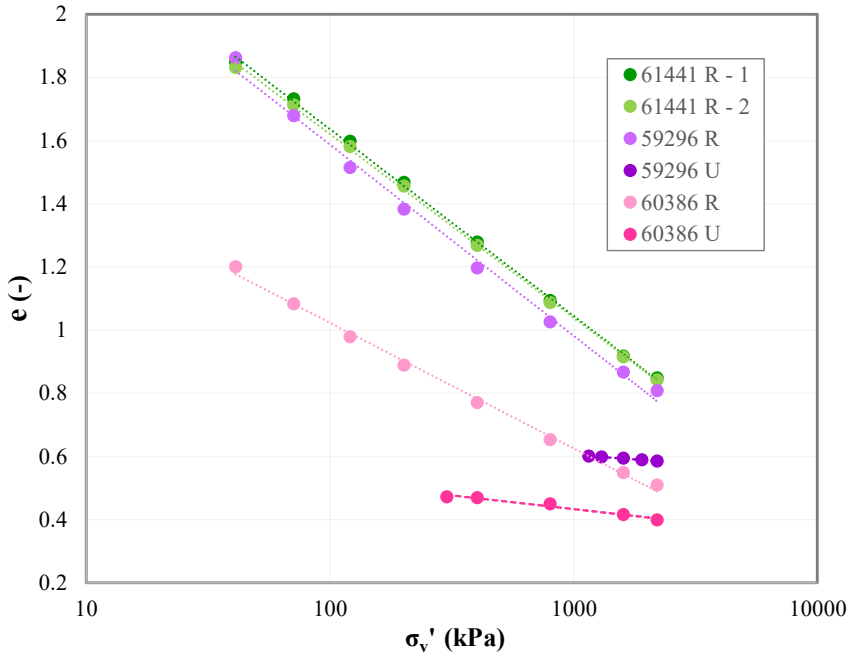

Fig. 7.3 Compression lines of one-dimensionally consolidated reconstituted (R) and undisturbed (U) samples.

The coefficients of consolidation c_v, determined using the log-time method, are listed in Table 7.2.

Table 7.2 Coefficients of consolidation (c_v) of reconstituted (R) and undisturbed (U) oedometer tests, given in m^2/year.

	59296		60386		61441	
Loading stage (kPa)	R	U	R	U	R - 1	R - 2
25	1.66	-	1.90	-	-	-
40	0.25	-	0.22	-	0.47	0.43
70	0.30	-	0.29	-	0.38	0.40
120	0.31	-	0.36	-	0.47	0.47
200	0.34	-	0.41	-	0.93	0.49
400	0.37	-	0.60	-	0.56	0.55
800	0.35	-	0.74	3.29	0.54	0.55
1600	0.33	1.32	0.84	2.73	0.42	0.39
1900	-	0.56	-	-	-	-
2200	0.29	0.84	0.78	2.54	0.19	0.29

Hydraulic conductivities, calculated from the coefficients of consolidation, are plotted in Fig. 7.4 against the mean effective stress on a logarithmic scale. Their trends, which are for the reconstituted samples almost identical, are demonstrated by power trendlines. However, sample 60386 shows the highest hydraulic conductivity again, despite its lowest void ratio.

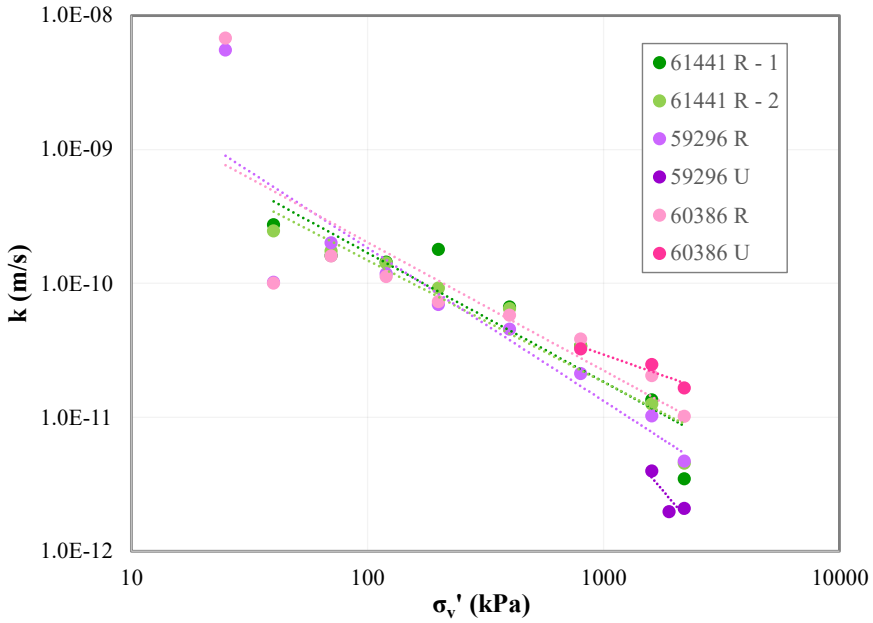

Fig. 7.4 Hydraulic conductivity of one-dimensionally consolidated reconstituted (R) and undisturbed (U) samples, calculated from c_v.

When the load steps are not double the previous ones, especially at low loads, the graphical detection of c_v using the log-time method is difficult to evaluate. Therefore, in Fig. 7.5, only the hydraulic conductivities calculated at the loading stages that are double the previous ones are presented. Again, sample 60386 shows a less steep decrease of hydraulic conductivity than the other two.

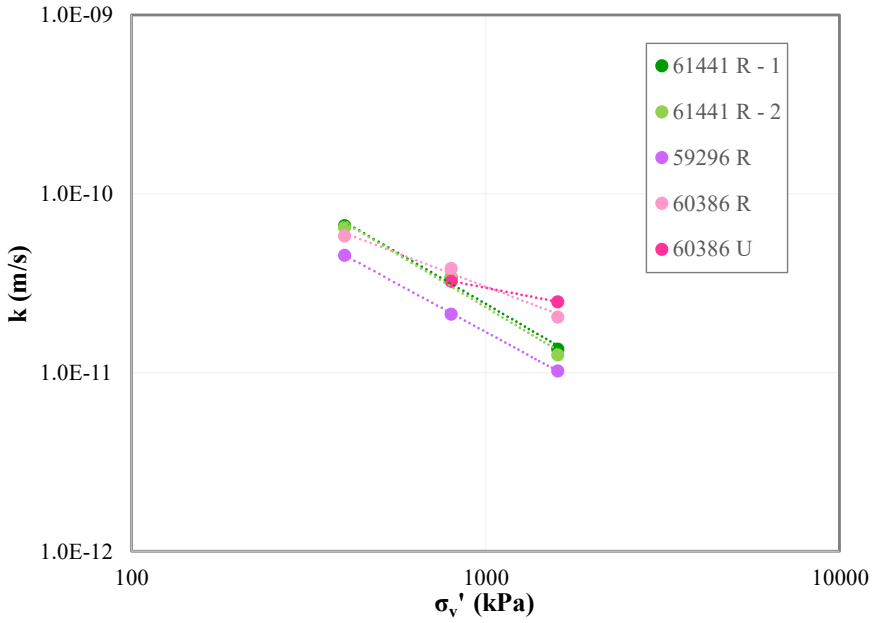

Fig. 7.5 Hydraulic conductivity of one-dimensionally consolidated reconstituted (R) and undisturbed (U) samples, calculated from c_v only at the loading stages that are double the previous ones.

8. Shear strength

For the determination of earth pressure at the rest K_0 from Jáky's equation (8), the knowledge of the critical strength represented by the critical state angle of friction φ'_{cr} (°) is necessary. K_0 is necessary for calculating the mean effective stress p' of oedometers and the multiplying factor f_{cv} discussed in chapter 5.5.1. For this purpose, two CIUP triaxial tests (Consolidated Isotropic Undrained with Pore pressure measurement) on the reconstituted samples were made. The first one on sample 60386 was done by the commercial laboratory SG Geotechnika a.s. I performed the other one on sample 61441.

The CIUP triaxial test is a standard laboratory test that measures the shear strength of soils. It is performed in the triaxial cell when the sample, consolidated to a given effective stress according to the procedure described in chapter 6.1, is axially loaded. Axial force, axial deformation, and pore pressure are recorded. Three identical reconstituted samples, consolidated to various pressures, are tested to obtain three different Mohr circles at failure, and consequently, a representative strength envelope. Its slope indicates the critical state angle of friction φ'_{cr} (°).

8.1. Sample preparation

The samples were prepared identically as in the case of isotropic compression. However, the sample's height was twice the height of the isotropic compression samples (7.6 cm). For the triaxial test, a side drain was used (see Fig. 8.1).

Fig. 8.1 Triaxial sample with side drain before testing.

8.2. Test procedure

The sample's saturation was verified by B-check and consolidated to effective pressures of 300, 600, and 900 kPa. From the consolidation course, the maximum shear velocity (at approximately 0.045 mm/minute) was calculated, and the velocity almost one order of magnitude slower (0.00645 mm/minute) was used to assure uniform distribution of pore pressure across the sample. After reaching 34 % of axial strain, the test ended, the sample was weighed and its volume under the water measured.

8.3. Data processing

From the height of the sample after the consolidation H_c (mm) and measured axial deformations ΔH, the axial strains ε_a (%) through the shearing stage were calculated as:

$$\varepsilon_a = \frac{\Delta H}{H_c} * 100 \tag{22}$$

The following variable, the deviator stress q (kPa), is defined as:

$$q = \frac{P}{A} * 1000 \tag{23}$$

where P (N) is the axial force measured by the load cell, and A (mm^2) the area of the sample's horizontal cross-section:

$$A = \frac{A_c}{100 + \varepsilon_a} * 100 \tag{24}$$

where A_c (mm^2) is the area after the consolidation.

The parameters of the Mohr circle (center, radius, and effective principal stresses) were calculated using the measured pore pressures u (kPa), and the calculated deviator stresses q (kPa): the minor effective principal stresses σ'_3 (kPa) as:

$$\sigma'_3 = \sigma_3 - u \tag{25}$$

where σ_3 (kPa) are minor principal stresses (cell pressure); the major effective principal stresses σ'_1 (kPa):

$$\sigma'_1 = \sigma'_3 + q \tag{26}$$

the centers of the effective Mohr circles s' (kPa):

$$s' = \frac{\sigma'_1 + \sigma'_3}{2} \tag{27}$$

and the radii of the effective Mohr circles t' (kPa):

$$t' = \frac{\sigma_1' - \sigma_3'}{2} \tag{28}$$

The highest ratio of t' and s' was found and the critical state angle of friction φ'cr (°) calculated for the one tested sample as:

$$\varphi_{cr}' = \sin^{-1}\left(\frac{t'}{s'}\right)_{max} \tag{29}$$

The resulting strength envelope is a tangent to the Mohr circles at the failure passing through the zero.

8.4. Test results

Unfortunately, the load cell measurement of the sample consolidated to 600 kPa was false; therefore, this sample was not included in the final evaluation. Fig. 8.2 shows the evolution of q and u with the increasing ε_a for the two valid samples.

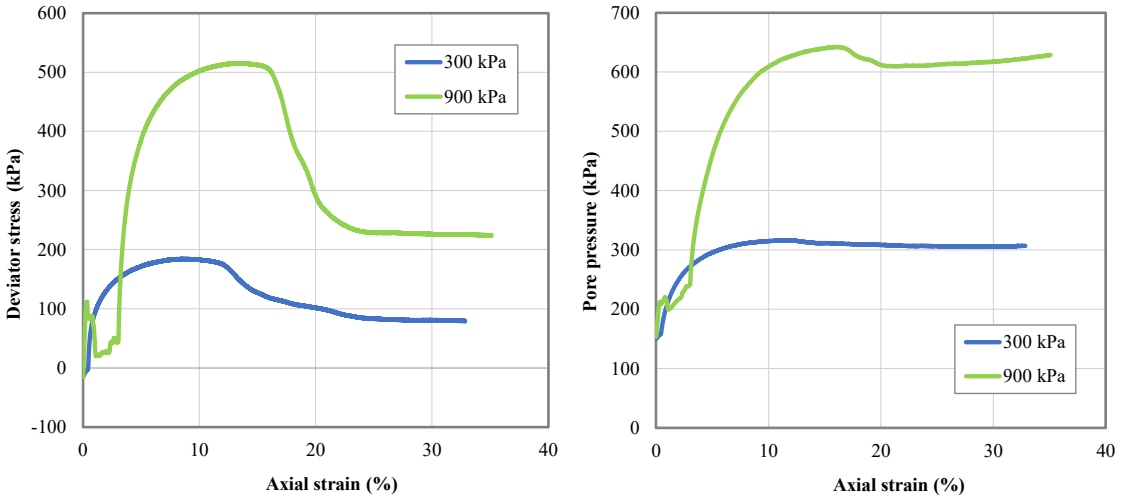

Fig. 8.2 Change of deviatoric stress q and pore pressure u with increasing axial strain ε_a during the triaxial test.

Fig. 8.3 graphically presents the triaxial test results of sample 61441. The stress paths show the course of *s'* and *t'* during the shearing. The resulting Mohr circles, and stress envelope, are presented too.

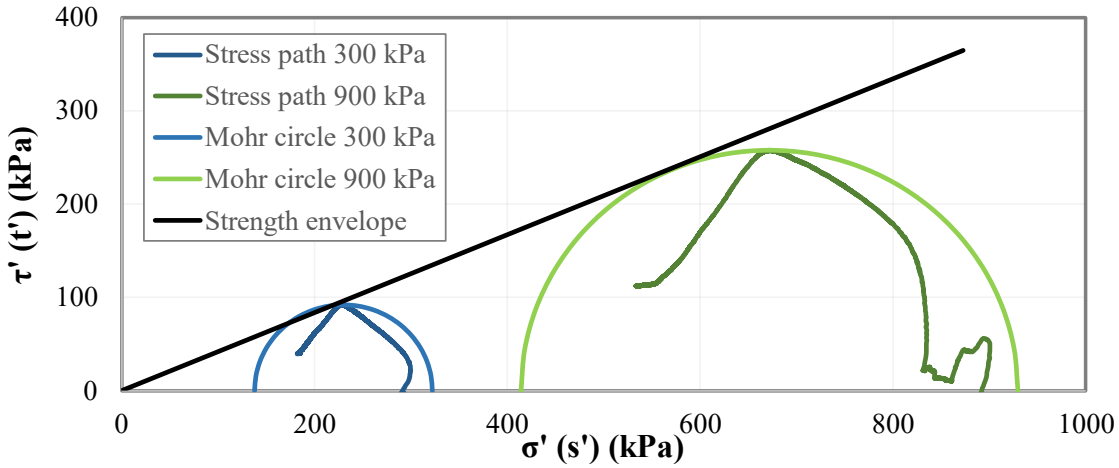

Fig. 8.3 Graphically displayed results of the sample's 61441 triaxial test.

The critical strength (φ'_{cr}) of sample 61441 is 22.8°. In the case of the sample 60386 determined by SG Geotechnika a.s., it is 22.3°. It confirms that the soils are very similar, thus being representative for comparison purposes. The critical strength of sample 59296 was not measured. However, values of the material parameters (grading curve and plasticity) of the sample lay between the values of parameters for the other two samples. Therefore, the critical strength value is expected to lay between their strengths, and it was estimated to be 22.5°.

9. Discussion

9.1. Saturation

The initial degree of saturation of models could not be determined before the testing due to their extremely soft structure. During the test, a small amount of air was coming out of the samples. Therefore, the initial degree of saturation is uncertain. However, the suction of model lumps measured after the test (Table 5.4) is more than an order of magnitude lower than the suction of the lumps at their natural water content when compared to the results determined in a study by Kostkanová (2011). Her study was related to a measurement of suction of the lumps sampled five months after their excavation. Moreover, the suction might have been caused by unloading the model at the end of the test. Such a small suction indicates the high degree of saturation in the presented models. In addition, the water contents of lumps and matrix in-between the lumps (Table 5.4) are practically identical, suggesting the full saturation of lumps.

A laboratory study, similar to that presented in this thesis, was carried out on the clays of Holešice Member by SG Geotechnika a.s. The full saturation of the physical models of a clay fill formed from Holešice clays had already been reached at the saturation phase following the identical procedure (J. Najser, personal communication). The different behavior may be explained by the difference in the materials of these two members. Holešice clays overlying the coal seam have a deltaic character, leading to their significant heterogeneity and a higher content of coarser material compared to the lacustrine clays of Libkovice Member. The coarser material results in a higher hydraulic conductivity. Hence, the water has easier access to the microvoids due to the lower air entry value.

9.2. Consolidation

The consolidation of both models is characterized by the absence of clear transition from primary to secondary consolidation (see semi-logarithmic charts in Fig. 5.9 and Fig. 5.10). The initial trend resembles the consolidation of a homogenous soil. However, its rate is significantly higher. It combines the relatively fast closing of the macrovoids and/or consolidation of the macrovoid fill accompanied by a significantly slower consolidation of lumps (linear charts in Fig. 5.9 and Fig. 5.10). When the macrovoids are approaching their full consolidation, the lumps are still consolidating, and

the overall consolidation gradually converts to creep. This structural behavior might explain the absence of a clear transition between primary and secondary consolidation, making the determination of testing time and c_v by the log-time method very difficult and uncertain.

Another feature that should be noted is the decreasing rate of consolidation with the increasing effective stress (see semi-logarithmic charts in Fig. 5.9 and Fig. 5.10). This trend can be especially seen for the first 15 hours after surcharge. As the macrovoids are closing, the hydraulic conductivity decreases, and the dissipation of the pore water pressure slows down.

9.3. Compressibility

The comparison of all determined compression curves is presented in Fig. 9.1. Sample 60386 from the inner fill shows a significantly lower position of compression curves and lower compressibility (except for the undisturbed sample) than the rest of the tested materials. The different position of all three tests performed on sample 60386 is consistent when compared to the corresponding tests on other materials and therefore, it can be assumed that the difference does not result from the incorrect measurement. The effect of the material offers the most plausible explanation. The mechanical characteristics, such as the grading curve or shear strength, show similar behavior of all tested materials. However, the plasticity shows some differences between sample 60386 (higher I_P and lower w_p) and the rest of the samples (see Table 4.1 and Fig. 4.4). Therefore, the lower position might be explained by the mineralogy of the samples. Kostkanová (2011) observed a similar phenomenon on clays from 3 mines, including the Bílina Mine. Their grading curves were similar, but their mineralogy and index properties differed. The difference in the mineralogy of the samples presented in this thesis would indicate that the monotonic sediments of Libkovice Member are not perfectly uniform from the mineralogical point of view. Unfortunately, no tests of the mineralogical composition of the samples were carried out. However, Müllerová (2017) determined the variation of montmorillonite content from 22 to 37 % on samples from only a 2.5 meters long drill core of the bottom part of Libkovice Member using the X-ray diffraction analysis. The possible lower content of montmorillonite in sample 60386 compared to other samples could partly explain this discrepancy as the montmorillonite binds more water in the crystal lattice than other clay minerals. This could result in an increase in porosity of identically graded samples for the same loading pressure. The compressibility

is then higher for the clays with a higher content of montmorillonite, which confirms the observations of Kostkanová (2011). The lowest compressibility and the highest hydraulic conductivity of sample 60386 (see Fig. 9.5) support this theory. On the other hand, the relatively high plasticity of sample 60386 (Fig. 4.4) does not confirm this explanation. Higher plasticity would be expected for a sample with a higher content of montmorillonite.

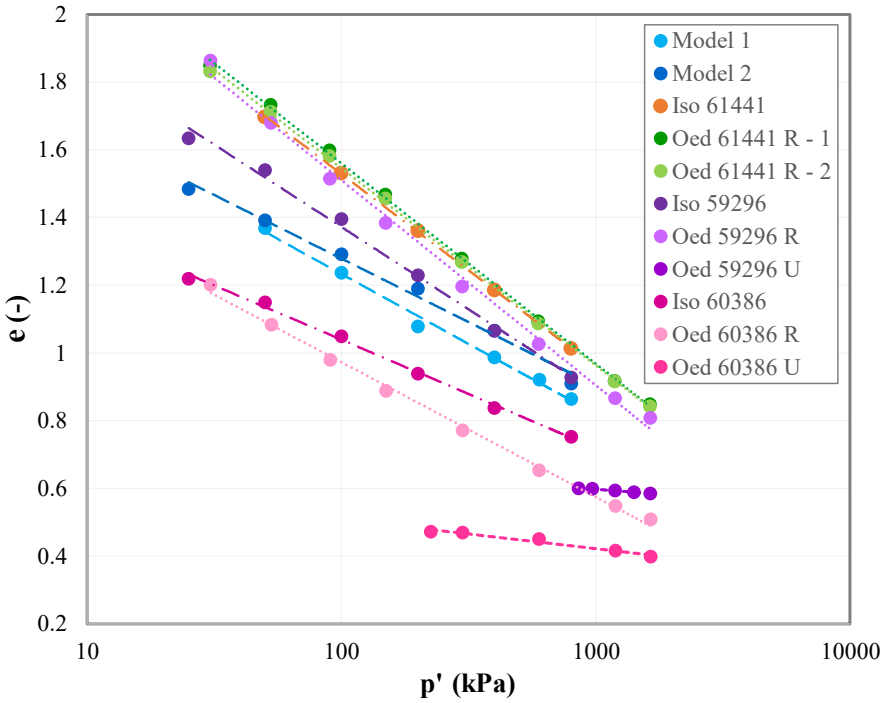

Fig. 9.1 Compression lines from all tests (Iso – isotropic compression, Oed – oedometric compression, R – reconstituted, U - undisturbed).

The relative position of each undisturbed sample to a corresponding NCL (compression line of the reconstituted sample), together with their low compressibility, demonstrate the significant overconsolidation of undisturbed samples, which agrees with their very stiff to hard initial consistency. The estimation of overconsolidation pressure of undisturbed samples 59296 and 60386 is presented in Fig. 9.2. For sample 59296, it is 4.9 MPa, and 4.2 MPa for sample 60386. Considering the unit weight of the saturated lumps to be 19 kN/m^3 above the water table and 9 kN/m^3 under the water table as used by Herbstová & Herle (2009), the highest depth of deposition of sample 59296 is estimated at 260 m and 545 m, respectively and for sample 60386 it is 220 m and 460 m, respectively. Taking into account the sampling depth of sample 59296 at 23 m, a considerable portion of denudation (as presented in chapter 3.1) can be assumed. On the contrary, the estimated depth of sample 60386 is smaller compared to sample 59296, even

though it was sampled significantly deeper (139 m). Also, its compressibility is higher. This disproportion can be explained by the fact that sample 60386 originates from the inner fill. Thus, the original clay was remolded, lost its original structure, and its compression curve does not reflect the geological history.

However, the estimation of maximum overburden is probably significantly affected by creep, and therefore the discussed depths are only indicative.

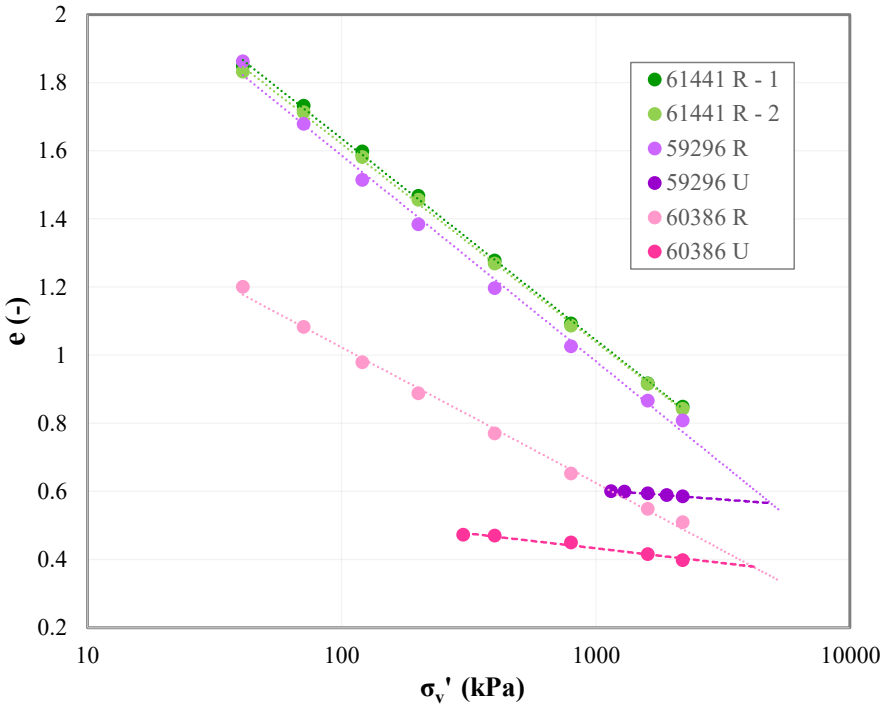

Fig. 9.2 Extended compression lines from oedometric tests (R – reconstituted, U – undisturbed).

As the literature review showed, the compression curves of a saturated clay fill should have a linear trend. The models presented in this thesis confirm this theory, as can be seen in Fig. 9.3. The results, corrected for a possible leakage (as discussed in chapter 5.6.1), are also displayed to demonstrate that the influence of correction is small. However, the main purpose of the figure is to present the theoretical limit void ratios of the model material at a given load. The upper limit representing the homogenous soil is the NCL from reconstituted samples. The lower limit representing the compressibility of the lump is defined by the compression line of an undisturbed oedometer sample 59296. Sample 59296 is used because no test on the undisturbed model material could be carried out, and its NCL is almost identical to the one representing the model's material. The difference between the compression line of the model and the undisturbed sample represents the influence of macrovoids. The compression line of the models lies between

the two limits. Therefore, in terms of compressibility, the clay fill behaves as a slightly overconsolidated soil. The previously mentioned analogical laboratory study on Holešice Member resulted in a similar relative position of the compression lines (J. Najser, personal communication).

Moreover, the extended compression lines of models in Fig. 9.3 (both original and corrected) cross the NCL approximately at the loading of 3 to 3.4 MPa (4 to 4.6 MPa of vertical effective stress). The results point out that up to the given effective stress, the clay fill's behavior is influenced by the macrostructure. Above this stress value, the clay fill would behave as a reconstituted soil. However, close to NCL, the compression line could be slightly curved. Therefore, the clay fill material might touch the NCL at higher pressures. This curvature could also influence the compression curves of undisturbed samples.

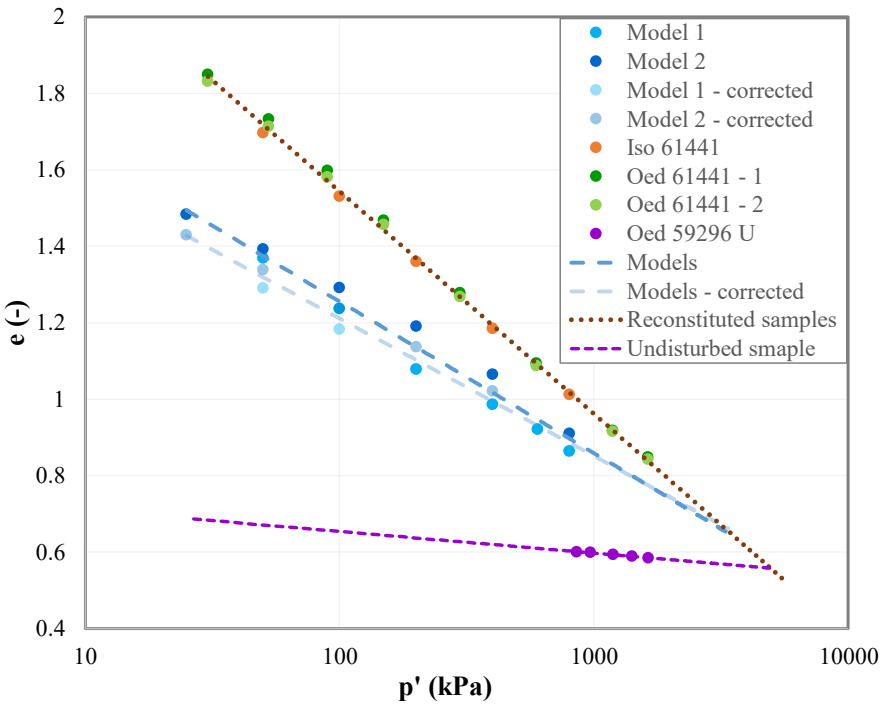

Fig. 9.3 Extended average compression lines of models (original and corrected), isotropic and oedometric compressions on reconstituted sample 61441, and extended compression line of undisturbed sample 59296.

9.4. Hydraulic conductivity

The determination of hydraulic conductivity calculated from c_v (oedometers) is indirect and less accurate. Therefore, the results calculated in this way are presented in

Fig. 9.4, being displayed by empty circles only. Notwithstanding, their trends are practically matching their isotropic equivalents.

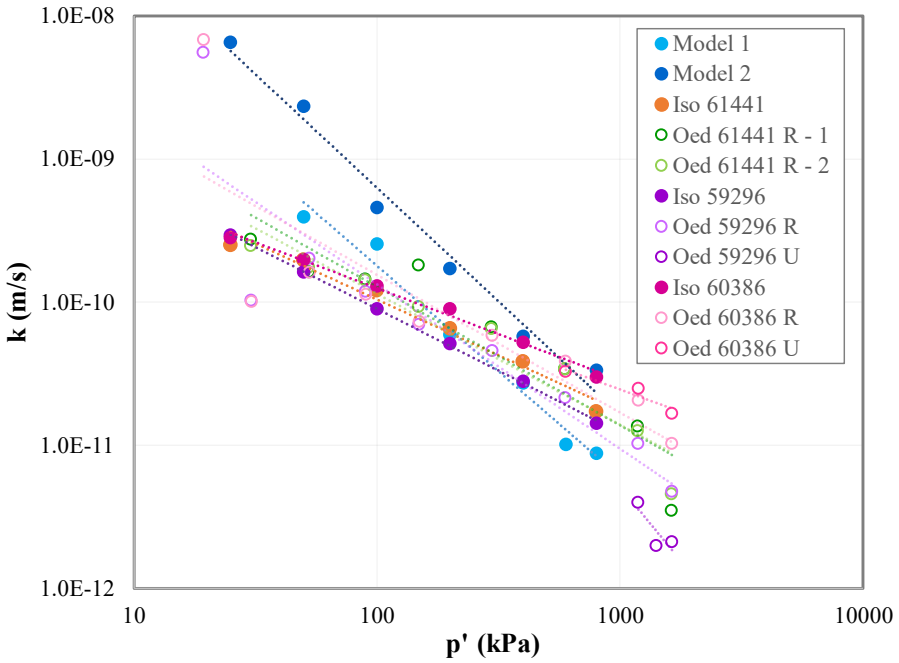

Fig. 9.4 Hydraulic conductivity from all tests (Iso – isotropic compression, Oed – oedometric compression, R – reconstituted, U - undisturbed).

As can be seen in Fig. 9.5, the decrease in hydraulic conductivity of a clay fill with increasing load is not linear on the logarithmic scale (unlike for the reconstituted soil). This non-linearity is caused by the gradual closure of macrovoids. The significant difference (approximately half an order of magnitude) between the hydraulic conductivities of both models might result from the difference in their testing duration (11 months model 1, 7 months model 2) and consequent creep. More significant creep results in a more significant macrovoid closure per consolidation stage, which causes a decrease in hydraulic conductivity. A contributing factor might be a slight difference in initial void ratios developed during the models' preparations. The mutual position of compression curves of both models (see Fig. 9.1) confirms these interpretations.

Kostkanová (2011) stated that the creep of lumps' contacts affects the hydraulic conductivity. Therefore, the longer the clay fill is loaded, the lower is its hydraulic conductivity; hence it cannot be considered a constant even for a given load.

The reason for the testing duration difference is the problematic determination of the end of the primary consolidation due to the unusual shape of consolidation curves and

considerable creep (mentioned above). Hence, the typical loading stage duration of the first model was 300 hours, while it took only 150 hours in the case of the second model.

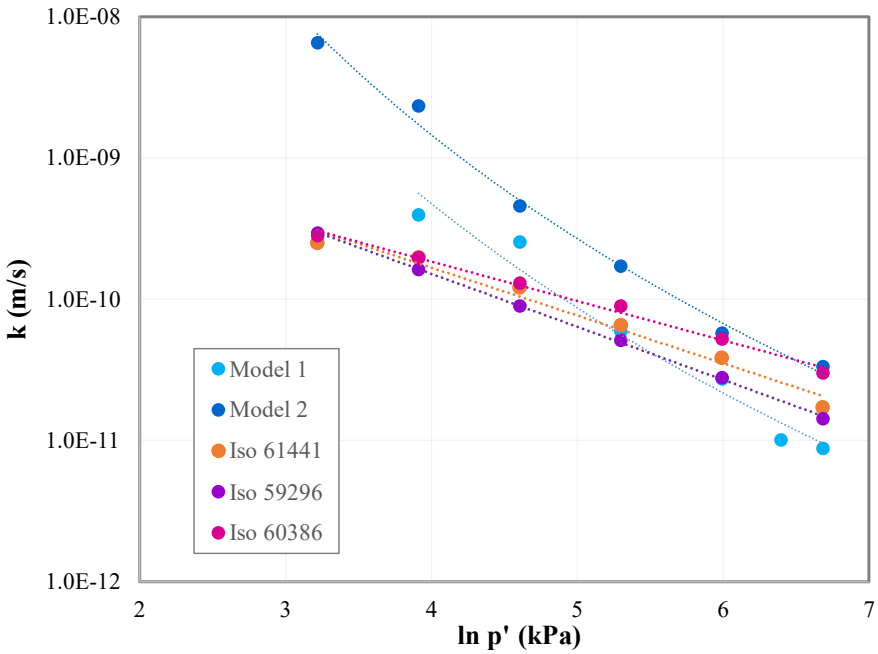

Fig. 9.5 Directly measured hydraulic conductivity of isotropically compressed samples (models and reconstituted samples – Iso).

The mean values for all the samples (as they are very similar) were calculated for each type of test (except the undisturbed oedometers) to obtain the general trends of hydraulic conductivity (see Fig. 9.6). The curve representing the models has a non-linear character gradually approaching the reconstituted soils and unifying at the mean effective stress of approximately 400 kPa. It corresponds to the vertical effective stress of about 540 kPa and 28 m thick overburden. At this point, the macrovoids close up, being filled with the reconstituted soil only, which then governs the clay fill's hydraulic conductivity. Karpíšková (2009) found the depth range of macrovoids closure from 12.5 m to 25 m. Najser, et al. (2010) detected it even shallower at 10 to 15 m, which is half the value presented in this thesis. However, the grading curve used for models' preparation by the aforementioned authors was significantly steeper than the curve presented in this thesis. Moreover, the lumps were softer in their studies; therefore, their models were more permeable, and the structure degradation was faster than in the case of this thesis.

The hydraulic conductivity calculated from c_v (oedometers) is displayed in Fig. 9.6 by a dashed line, as the indirect determination implements some uncertainties (for

example, using K_0 to get p') into the calculation. Nonetheless, the hydraulic conductivity of oedometers is practically identical to the isotropically compressed reconstituted samples.

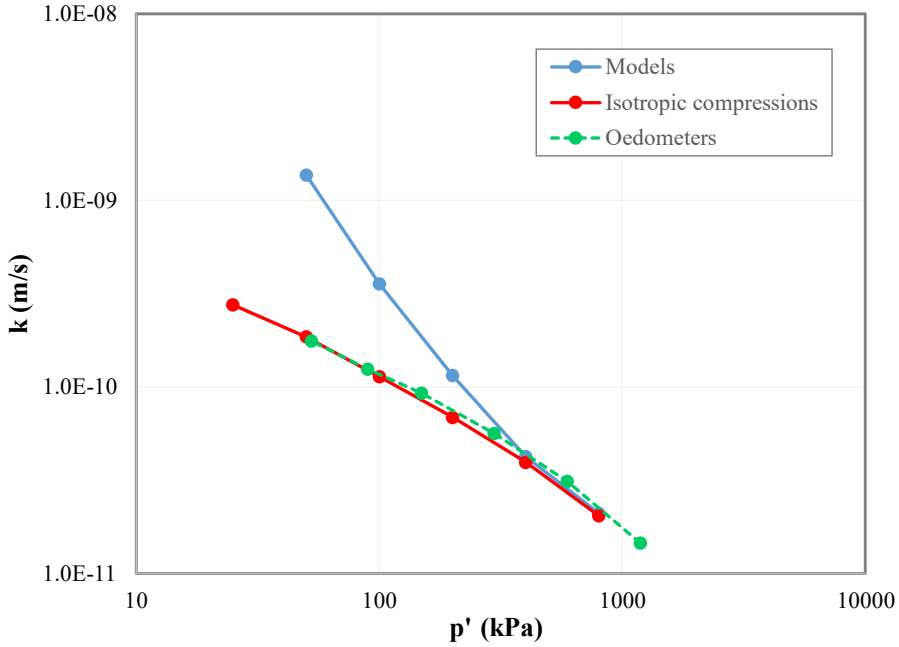

Fig. 9.6 Mean values of hydraulic conductivity from all samples for each type of test except the undisturbed oedometers.

9.5. Summary

The results show that the clay fill is approaching the hydraulic conductivity of a reconstituted soil at approximately 540 kPa of the vertical effective stress, while the compressibility of a reconstituted soil is reached at the range between 4 and 4.6 MPa. This suggests that the macrovoids are firstly filled with the reconstituted soil, and therefore do not work as the preferential paths for water anymore. However, the lumps are still present in the structure and affect the compressibility up to significantly higher pressures. The confirmation of these findings can be given by the occurrence of lumps in the structure of models after compression at 800 kPa (see Fig. 5.7 c and d).

10. Conclusion

The results confirm that the stress applied to the clay fill is an important factor governing the change of its structure. The behavior of a saturated clay fill, as examined by the scaled-down physical models, is in line with the observations seen in the literature review. The tests carried out within the scope of this thesis confirmed that both the compressibility and hydraulic conductivity represent suitable parameters for analysis of clay fill structural transformation.

During the consolidation of the clay fill, the structural behavior is very complex when compared to the consolidation of a homogeneous clay. Its consolidation curves do not have the shape usually determined in a reconstituted soil. The excess pore pressures dissipate first in macrovoids while the dissipation in lumps continues, and the overall consolidation then progressively converts to creep. Therefore, the transition from primary to secondary consolidation is practically indistinguishable. Furthermore, the consolidation curves of models demonstrated that the rate of consolidation significantly decreases with increasing loading pressure as the macrovoids close.

The study of models' compressibility confirmed the linearity of the compression curve of a saturated clay fill on a semi-logarithmic scale. Moreover, its position was observed between the limits given by the NCL of a reconstituted clay and the compression line of the overconsolidated lump. Up to the vertical effective stress range of 4 to 4.6 MPa, the saturated clay fill behaves as a slightly overconsolidated soil. At higher stresses, the limiting compression lines merge, the influence of the macrostructure diminishes, and the clay fill behaves as a reconstituted soil.

As the macrovoids close with increasing pressure, the hydraulic conductivity of the clay fill decreases non-linearly. The complete closure of macrovoids is reached at about 540 kPa of the vertical effective stress. At higher stresses, the macrovoids are filled with the reconstituted soil only, which then governs the hydraulic conductivity. The trend becomes linear, and the hydraulic conductivity is the same as for the reconstituted soil.

Moreover, a significant effect of creep was observed on the models during testing. After the end of primary consolidation, void ratio and hydraulic conductivity gradually decrease in time. Therefore, the applied stress should not be considered the only variable when evaluating the structural changes of a clay fill.

11. References

ASTM. (2003). Standard Test Method for Measurement of Soil Potential (Suction) Using Filter Paper. *D 5298-03*. ASTM.

Atkinson, J. (2007). *The Mechanics of Soils and Foundations* (2nd ed.). Taylor & Francis.

Cotecchia, F., & Chandler, J. (2000). A general framework for the mechanical behaviour of clays. *Géotechnique, 50*(4), 431-447.

Cox, D. (1979). Volume change of compacted clay fill. *Clay Fills Conference*, (pp. 79-86). London.

Dortland, A. (2019). *A study into the closure of the interlump voids of a mechanically dredged stiff clay fill.* Master's Thesis, Delft University of Technology.

Feda, J. (1982). *Mechanics of Particulate Materials - The Principles.* Amsterdam-Prague: Elsevier-Academia.

Feda, J. (1998). Fragmentary clay - a difficult waste material. *Engineering Geology*(51), pp. 77-88.

Head, K. (1994). *Manual of Soil Laboratory Testing* (2nd ed., Vol. 2). New York - Toronto: John & Sons, Inc.

Head, K. H. (1998). *Manual of Soil Laboratory testing* (2nd ed., Vol. 3). John Wiley & Sons Ltd.

Herbstová, V., & Herle, I. (2009). Structure transitions of clay fills in North-Western Bohemia. *Engineering Geology*(104), pp. 157-166.

Hurník, S. (1978). Reconstruction of the thickness of the Overlying Complex in North Bohemia Brown-coal Basin (Miocene). (in Czech). *Journal for Geology and Mineralogy, 23*(3), 265-276.

Charles, J. (2008). The engineering behaviour of fill materials: the use, misuse and disuse of case histories. *Géotechnique, 58*(7), 541-570.

Jáky, J. (1948). Pressure in Silos. *2nd International Conference on Soil Mechanics and Foundation Engineering*, *1*, pp. 103-107. Rotterdam, Nederland.

Jun Wei, Y. (2004). *Consolidation Characteristics of Lumpy Fill.* PhD Thesis, National University of Singapore.

Juneja, A., & Chafale, A. S. (2018). Consolidation behaviour of double-porosity clay using flexible wall permeameter. *Ground Improvement*, 1-13.

Karpíšková, M. (2009). *Porosity and permeability of a clayfill model (in Czech).* Master's Thesis, Charles University in Prague, Faculty of Science, Prague.

Karthikeyan, M., Dasari, G. R., & Tan, T.-S. (2004). In situ characterization of land reclaimed using big clay lumps. *Canadian Geotechnical Journal, 41*, 242-256.

Kostkanová, V. (2011). *Mechanical Behaviour of Variably Saturated Clay Fills.* PhD Thesis, Charles University in Prague, Faculty of Science, Institute of Hydrogeology, Engineering Geology and Applied Geophysics, Prague.

Kostkanová, V., Herle, I., & Boháč, J. (2014). Transitions in structure of clay fills due to suction oscillations. *Procedia Earth and Planetary Science*(9), pp. 153-162.

Kvaček, Z., Böhme, M., Dvořák, Z., Konzalová, M., Mach, K., Prokop, J., & Rajchl, M. (2004). Early Miocene freshwater and swamp ecosystems of the Most Basin (northern Bohemia) with particular reference to the Bílina Mine section. *Journal of the Czech Geological Society*(49), pp. 1-40.

Leung, C., Wong, J., Manivanann, R., & Tan, S. (2001). Experimental Evaluation of Consolidation Behavior of Stiff Clay Lumps in Reclamation Fill. *Geotechnical Testing Journal, 24*(2), 145-156.

Li-Ang, Y. (2003). *Mechanics of the Consolidation of a Lumpy Clay Fill.* PhD Thesis, National University of Singapore.

Mach, K. (2002). *Anomalous structures of main brown-coal seam of the Most Basin in the area of the Bílina Delta (Miocene, Czech Republic).* PhD Thesis, Charles University in Prague, Prague.

Mapy.cz. (2019). Retrieved March 8, 2021, from https://mapy.cz/letecka?x=13.7160985&y=50.5702188&z=14

Mašín, D. (2007). A hypoplastic constitutive model for clays with meta-stable structure. *Canadian Geotechnical Journal, 44*(3), 363-375.

Müllerová, E. (2017). *Chemostratigraphy of the Holešice Member in the Most Basin (Miocene) (in Czech).* Master's thesis, Charles University in Prague, Prague.

Najser, J. (2010). *Modelling of Lumpy Clay Fills.* PhD Thesis, Charles University in Prague, Prague.

Najser, J., Mašín, D., & Boháč, J. (2012). Numerical modelling of lumpy clay landfill. *International Journal for Numerical and Analytical Methods in Geomechanics, 1*(36), 17-35.

Najser, J., Pooley, E., Springman, S., Laue, J., & Boháč, J. (2010). Mechanisms controlling the behaviour of double-porosity clay fills; in situ and centrifuge study. *Quarterly Journal of Engineering Geology and Hydrogeology, 43*, 207-220.

Rajchl, M., Uličný, D., & Mach, K. (2008). Interplay between tectonics and compaction in a rift-margin, lacustrine delta system: Miocene of the Eger Graben, Czech Republic. *Sedimentology, 55*(5), 1419-1447.

Robinson, R., Tan, T., Dasari, G., Leung, C., & Vijayakumar, A. (2005). Experimental Study of the Behavior of a Lumpy Fill of Soft Clay. *International Journal of Geomechanics, 5*(2), 125-137.

Rowe, P. W. (1959). Measurement of the Coefficient of Consolidation of Lacustrine Clay. *Géotechnique, 9*(3), 107-118.

Shi, X., & Herle, I. (2014). Laboratory investigation of artificial lumpy materials. *Engineering Geology, 183*, 303-314.

Shi, X., Herle, I., & Wood, D. (2017). A consolidation model for lumpy composite soils in open-pit mining. *Géotechnique*, 1-16.

Skempton, A. W. (1954). The Pore-Pressure Coefficients A and B. *Géotechnique, 4*(4), 143-147.

Yang, L., Tan, T., Tan, S., & Leung, C. (2002). One-dimensional self-weight consolidation of a lumpy clay fill. *Géotechnique, 52*(10), 713-725.